EURASIAN JOURNAL OF MATHEMATICAL
AND COMPUTER APPLICATIONS
ISSN 2306–6172
Volume 13, Issue 2 (2025) 13 – 42

THE DIRECT AND INVERSE PROBLEMS OF MODELING THE CARBON BLACK FURNACE PRODUCTION PROCESS

Cherny S.G., Zeziulin I.V., Tarraf D., Pochuev A.P., Boronenko I.S. [1]

Abstract To establish the influence of hydrocarbon raw materials composition, duration and temperature of a reaction on the dispersion and structural properties of the carbon black produced in a reactor, two numerical three-dimensional models for the reactor operation process are proposed. These models are made in the approximation of the Eulerian-Eulerian approach and implemented on the FlowVision PC and ANSYS PC platforms. In the FlowVision model a convection-diffusion equations for the dispersed phase are used. In ANSYS PC, the movement of the dispersed phase is described by the Navier-Stokes equations. The article also analyzes a model for describing the nucleation and growth of carbon black particles. The Moss-Brookes model of uncontrolled formation of soot particles during acetylene combustion was taken as the basis for the model of carbon black formation in the reactor. To generalize it to carbon black production in a reactor under harsh pyrolysis conditions at a temperature no lower than 1000 °C and a high degree of reactions heterogeneity, a number of techniques are proposed. The numerical results of modeling the spray atomization and evaporation of raw materials processes in the reactor are presented. The sensitivity of the mass and carbon black particles quantaty on the constructed model input parameters was analyzed.

Key words: Carbon black formation, Soot formation, Eulerian - Eulerian approach, CFD, ANSYS PC, Flow Vision PC, Spray atomization, evaporation.

AMS Mathematics Subject Classification: 35Q30, 35Q70, 65M06,76F25, 76T10, 76T30.

DOI: 10.32523/2306-6172-2025-13-2-13-42

1 Introduction

1.1 Characteristics of carbon black

Carbon black, the production modeling of which this article is devoted to, is one of the types of soot [1]. Soot is a highly dispersed product of incomplete combustion or partial decomposition of hydrocarbons contained in natural gases or petroleum feedstocks. Soot consists of at least 90% carbon. Soot formation occurs during the decomposition of hydrocarbons under the influence of high temperature and the release of carbon in the form of soot. To obtain soot, various types of raw materials are used: technical anthracene; coal (anthracene) oil; green oil; coke distillate; natural distillation; petroleum pyrolysis gas; acetylene. The most important physicochemical properties of soot are the degree of dispersion, the nature of secondary structures (soot chains) and the surface properties of soot particles. The degree of soot dispersion is usually characterized by the arithmetic mean value of the soot particles diameter. Each type of soot consists of particles of different sizes. The specific surface of soot is directly related to the degree of dispersion. The smaller the soot particle size, the larger its specific surface. The degree of dispersion affects many properties of soot, primarily its enhancing effect on rubber, since the magnitude of the adsorption forces that bind soot to rubber depends on the size of the specific surface of the soot. The carbon black used in the production of rubbers and plastics, is created from liquid hydrocarbon raw materials by heating it [2].

---

[1] Corresponding Author.

The structural elements of carbon black are flat lattices consisting of six-membered carbon cycles [3]. Approximately 3-7 such flat lattices, located not exactly one above the other, but shifted relative to each other, form an elementary crystallite. The primary particle of carbon black is formed by randomly but compactly arranged elementary crystallites. When carbon black is formed during the growth of particles, their collisions occur, as a result of which they can grow together, forming strong aggregates called primary units. The presence of primary aggregates, their size and shape determine the property of carbon black (called structural properties). The degree of development of the structure chain, depends on the method of obtaining carbon black and raw materials. The furnace production method is especially favorable for the formation of primary units. When the primary structures come into contact, they form secondary units, the degree of strength depends on the intermolecular bonds (from weak van der Waltz bonds to relatively strong hydrogen bonds). Another characteristic of carbon black is its dispersity. As noted above, the degree of dispersion is characterized quantitatively by the average particle diameter, specific surface, and also by the specific number of particles in soot. The smaller the particles, the higher the dispersity and, conversely, the larger the particles, the less dispersity.

The most common method for producing carbon black is the furnace method, in which carbon black is produced by the oxidative decomposition of liquid hydrocarbon raw materials at a temperature of 1100-1900 °C , achieved by burning natural gas in the combustion chamber of the reactor. In [4] it is shown that technological conditions and the hydrocarbon composition of the raw material determine the main indicators of the quality of the dispersed product (dispersity, structural properties) Establishing the relationships between the composition of hydrocarbon raw materials, temperature, reaction time and the quality of carbon black (dispersity, structural properties) is the main task, the solution of which makes it possible to optimize the technical and economic characteristics of the entire process. The most difficult stage of this process is the spray atomization of raw materials into a flow of heat-carrier gas. It is necessary to achieve the specified degree of fineness of the atomization of the raw material and the uniform distribution of the droplets, which would ensure its complete evaporation before the start of pyrolysis and the desired carbon structural properties. In this case, the likelihood of coke formation contaminating the product will be minimal [4].

1.2 Models of spray and evaporation of liquid hydrocarbons in the reactor

Due to the complexity of experimentally studying the processes occurring in the production of carbon, mathematical modeling plays a key role in improving its quality. In [5-7], two alternative variants of a comprehensive numerical model of this process are proposed. Both variants of the model describe in three-dimensional formulation the spray and evaporation of liquid hydrocarbon raw material in the gas-heat carrier flow and are implemented using the Eulerian-Eulerian approach [72], realized in [5, 6] on the FlowVision PC, and in [7] on the ANSYS PC. In both variants, the movement of the carrier phase (gas-heat carrier and evaporation products of the raw material) is described by the Navier-Stokes equations. To describe the dynamics of the dispersed phase in FlowVision PC, convective-diffusive equations are used for the concentration of particles, momentum, and energy of the phase [5, 6]. One of the advantages of the model on the FlowVision PC is its greater efficiency compared to the model on the ANSYS PC. In ANSYS PC, the movement of the dispersed phase, like the carrier phase, is described by the Navier-Stokes equations [7], which require significantly more time for their solution. A disadvantage of the model on the FlowVision PC is the need to specify the already atomized raw material at the entrance to the computational area of the dispersed phase through the nozzle. In fact, the model built on the FlowVision PC does not describe the atomization of the raw material from the nozzle. It only describes the further

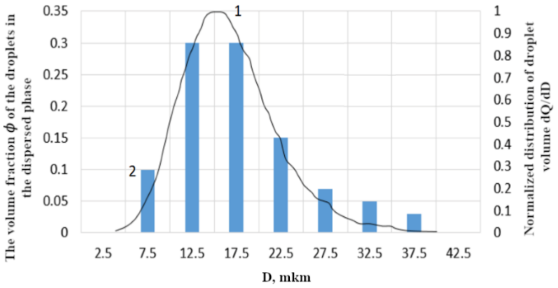

Figure 1: Droplet size spectrum at the nozzle: 1 – diameter distribution function of droplets obtained experimentally; 2 – selection of values for FlowVision PC calculation.

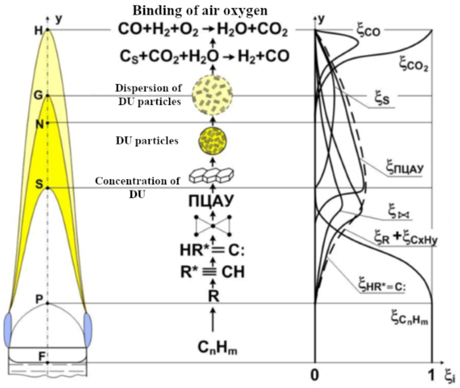

Figure 2: The process of soot formation in LDF [41]: ξ_i – fraction of carbon in the i-th state; S – DC (dispersed carbon); R – radicals; C_xH_y – newly formed hydrocarbons.

evolution of the aerosol of the raw material launched through the nozzle into the reactor. The initial spray state at the nozzle must be set. That is, it is necessary to specify the spray mode, the parameters of which are the input data of the process modeling task on the FlowVision PC. What needs to be determined at the nozzle output before starting the calculation? What is needed: the number of droplet families, each with its specific droplet diameter (discrete distribution of droplet diameters - droplet size spectrum); the volume fraction of droplets of a given diameter, and the concentrations of droplets in each family. It should be noted that in this task, the initial (starting) spray mode of the raw material is only needed as a boundary condition for the model - the further evolution of the spray process, including droplet breakup and coalescence, is well described by the model. The problem of specifying the spray parameters of the raw material at the nozzle is usually solved based on experimentally obtained data on the volume distribution of droplets by diameter D, normalized to its maximum value $Q(D)$ (Fig. 1).

The velocity of the dispersed phase (droplets) V_d m/s at the inlet is known from the physical formulation of the problem. The volume fraction of the raw material phase at the inlet is determined taking into account the velocity V_d and the flow rate. The experimentally determined volume distribution function $\frac{dQ}{dD}$ occupied by droplets with a diameter D and normalized to its maximum value is shown in Fig. 1 as a solid line, and its values are presented on the right side of the graph. N_{di} - the number of droplets with a diameter d_i in the size spectrum, for which the value $\frac{dQ}{dD}(d_i)$ is calculated. The volume fraction ϕ_i of droplets with a diameter d_i in the dispersed phase is calculated.

$$\phi_i = \frac{dQ}{dD}(d_i) \Big/ \sum_{i=1}^{N_d} \frac{dQ}{dD}(d_i), \tag{1}$$

where, formula (1) ensures the condition $\sum_{i=1}^{N_d} \phi_i = 1$ is met. The values of the volume fractions and the corresponding droplet diameters in the droplet size spectrum of the raw material at the input are given in table. Also, Fig. 1 shows the histogram illustrating the discrete distribution of droplet diameters chosen for the calculation in FlowVision PC. At the raw material input (dispersed phase) into the reactor, its volume fraction α is set. Given the feed rate of the raw material from the atomizer $V_d = 10$ m/s, the volume fraction α is calculated by the formula:

$$\alpha = \frac{Q_d}{\rho_d(T_d) \cdot V_d \cdot S}$$

where Q_d is the raw material flow rate, and S is the area of the atomizer outlet, taken from the physical problem statement.

Based on α, as well as the distribution ϕ_i depending on d_i, the concentration value of droplets in each family (set) $n_{d,i}$ at the raw material input is determined from the concentration equation:

$$n_{d,i} = \alpha \cdot \frac{\phi_i(d_i)}{V(d_i)}, \tag{2}$$

where $V(d_i)$ is the volume of a droplet with diameter d_i. In this model, it is assumed that all droplets are spheres with a diameter d_i. The equations for particle concentration, momentum, and phase energy are solved separately for each family i of particles.

It should be noted that when solving this problem using the Eulerian-Lagrangian approach, from equation (2), the number of raw material droplets N_i in each family (set) corresponding to the current diameter d_i from the specified spectrum of raw material droplet sizes entering per unit time is found:

$$\frac{dN_i}{dt} = n_i \cdot V_d \cdot S = \alpha \cdot \frac{\phi_i(d_i)}{V(d_i)} \cdot V_d \cdot S \tag{3}$$

Table 1: Model constants of the problem, their dimensions and values

Family number, i	1	2	3	4	5	6	7
Diameter of family particles d_i, μ m	7.5	12.5	17.5	22.5	27.5	32.5	37.5
Family volume fraction in the phase ϕ_i	0.1	0.3	0.3	0.15	0.07	0.05	0.03

The model built on the ANSYS PC does not have the problem of defining the initial stage of raw material atomization. In ANSYS PC, the movement of the dispersed phase, as well as the carrier phase, is described by the Navier-Stokes equations [7], which can adequately describe the initial stage of the raw material atomization process based only on general data - the raw material feed rate and its physical parameters.

In [8], an attempt is made to take the next step in constructing a complete closed model of reactor operation - a concept of a model for the formation of carbon black is proposed, closing the chain of processes it models: “raw material atomization - evaporation of atomized raw material - nucleation of carbon black particles in raw material vapors”. The present work continues the research started in [8] on the construction of a carbon black output model, its verification, and validation.

1.3 Models of soot and carbon black formation

In most studies concerning the modeling of carbon formation, the models describes the nucleation and development of soot under uncontrolled conditions. Usually in a free burning flame. For example, as in [9] it has been described the formation of carbon soot in a flame of burning acetylene. Distinctive features of the process of producing carbon black in a reactor are the harsh conditions of pyrolysis, which carried out at a temperature no lower than 1000°C and a high degree of reaction heterogeneity, the raw material is fed into the reactor as liquid, it evaporates, and then forms a solid (carbon black) [10]. Therefore, one of the goals of the presented work is to generalize the model of uncontrolled soot formation during the combustion of hydrocarbon raw materials to the model of carbon black formation in a reactor. The general concept of soot formation models can be found in [11-13]. It can be formulated as follows: aromatic hydrocarbons are formed in the gaseous environment obtained after the combustion of non-aromatic fuel. Their structure is complicated by the successful addition of alkyl groups. After reaching a certain size, the soot particle “condenses”. Subsequently, the growth of soot particles continues under the influence of the processes of coagulation, agglomeration and surface growth. In the simplest approach, it is assumed that the process of soot formation is constant and depends on the composition of a particular fuel. In this case, the volume fraction of soot is associated with the local value of the mixture fraction. The ratio of gaseous phase components in laminar and turbulent flames extends to the concentration of solid soot particles [14-17]. It is assumed that soot formation occurs close to stoichiometry and that it subsequently dissipates in the flow [18-22]. In [23], for the concentrations of radical nuclei and soot particles, two equations are solved that describe the formation of elementary soot particles and their growth. This approach was developed in [24], which takes into account soot burnout using a vortex model of gaseous combustion, and in [25] for simulating a fire in a swimming pool. Model [23] was applied in [26] for a full-scale explosion simulation in a multi-room facility. The numerical results matched the real data quite well. Further development of soot formation models based on two equations was carried out in [27-30]. These models take into account the physical and chemical processes that occur during the formation of soot particles from the active medium, the growth of soot particles due to the addition of elementary particles, and the combination of small particles into larger ones. A detailed account of chemical processes is carried out in the model [31] for the gaseous phase of a hydrocarbon mixture. This model describes the ongoing chemical processes in the presence of a pyrolysis product such as acetylene. The latter is important for correct prediction of the process of formation of carbon particles. Simplified chemical mechanisms of the behavior of heavy hydrocarbons and heterogeneous fuels are studied in [32,33,34].

In order to reasonably simplify the model being created, we will consider acetylene to be the main source of elementary carbon particles involved in the processes of formation and surface growth. In this case, we will take into account that chemical reactions during the pyrolysis of liquid hydrocarbons proceed much more slowly than reactions during the combustion of acetylene. We will take into account the modification of the Brooks-Moss model considered in [30-33], that describes the combustion process of kerosene fuel, which affects the formation of carbon particles.

1.4 Models of soot and carbon black formation in the ANSYS PC

We will separately list the models of nucleation and growth of carbon particles available in the commercial ANSYS software. Two empirical models predict soot concentrations in combustion systems: the one-step model by Khan and Greaves [35] and the two-stage model by Tesner [36, 37]. The combustion of soot is assumed to be determined according to Magnussen [36]. The Moss-Brooks model [38] is less empirical and should theoretically provide better accuracy than the models by Khan, Greaves, and Tesner, describing the formation of soot in a methane flame in ANSYS. The Hall extension of the Moss-Brooks model [39] is applicable to fuels with higher hydrocarbon content, such as kerosene. Finally, the method of moments [40] considers the soot size distribution, where the diameters of the soot particles change dynamically, using fewer empirical constants to model various mechanisms of soot formation.

1.5 The nucleation and growth of soot particles as a Markov process of carbon transitions between defined states

In [41], an original and rather ingenious mathematical model of the nucleation and growth of soot particles is proposed. The process of soot formation in a laminar diffusion flame (LDF) is represented as a chain of separate stages of hydrocarbon fuels (HCF) transformation and its states [42,43,44]: 1) formation of radicals, and then carbene-type biradicals during fuel pyrolysis; 2) formation of polycyclic aromatic hydrocarbons (PAH); 3) formation of PAH dimers; 4) formation of soot crystallites; 5) formation and growth of soot particles. The presented chain of soot particle transformations is shown in Fig. 2. Transverse convective transfer of substances in LDF is absent. Therefore, it is assumed that the chain of carbon transformations in LDF during HCF combustion is implemented in the same way in all elementary flow tubes, as in the axial flow tube passing through points F, P, S, N, G, and H in Fig. 2. The transformations occurring are very complex and multi-stage, involving a huge number of different compounds, mainly short-lived ones, many of which cannot be registered by known physical methods. Therefore, the processes under consideration cannot currently be fully described using classical chemical kinetics. In [41], the nucleation and growth of soot particles in LDF during HCF combustion are presented as a Markov process and described by the Kolmogorov system of ordinary differential equations (ODE), the solution of which is a set of functions representing the probabilities of finding carbon in the defined states. When deriving the relations for carbon transition frequencies between defined states, approaches adopted in molecular kinetics, as well as concepts of the mechanisms of soot particle formation and growth processes, obtained from the analysis of experimental research results under LDF conditions, were used. Using the obtained ODE system, numerical modeling of the mentioned processes in LDF of iso-octane, toluene, and a mixture of iso-octane and toluene in a 1:1 ratio at a combustion regime close to the smoke point threshold was carried out. Good agreement between the calculation results and experimental data for LDF of toluene was obtained.

1.6 Generalization the model of uncontrolled soot formation during the combustion of hydrocarbon raw materials to the model of carbon black formation in the reactor

The model considered in [8] is based on two ordinary differential equations with source terms describing the instantaneous formation of densities of two carbon quantities: the number of particles N and their mass M [9]. The model contains the mechanisms of carbon formation and development. These are nucleation (formation of particles due to the condensation of carbon from the evaporation products of raw materials), coagulation (adhesion of small particles to form larger ones), surface growth (attachment of individual atoms and radicals to the surface of large particles) and oxidation (reactions with oxygen and OH radicals). The model coefficients, established separately for each source term responsible for the specified mechanisms, after their summation the final form of the model is determined. These coefficients in our case depend on the flow parameters in the reactor, the mixture of raw materials, its evaporation products and heat-carrier gas. For example, as in [9], the model under consideration is used to describe the formation of carbon soot in a flame of burning acetylene. Distinctive features of the process of producing carbon black in a reactor are the harsh conditions of pyrolysis, which carried out at a temperature no lower than 1000 °C and a high degree of reaction heterogeneity, the raw material is fed into the reactor as liquid, it evaporates, and then forms a solid (carbon black) [10]. Therefore, one of the goals of the presented work is to generalize the model of uncontrolled soot formation during the combustion of hydrocarbon raw materials to the model of carbon black formation in a reactor. For generalization, two approaches are possible.

1.6.1 Stoichiometric laws of carbon black formation in a reactor

In this approach [1,10,45], to construct a mathematical model, stoichiometric laws are used – the equations of material and heat balance. These equations involves: the amount of gas and feedstock supplied to the reactor; chemical composition of gas and raw materials. From the equation, the amount of air required for the process is determined, as well as the amount of soot and gaseous products that are obtained during soot formation. In the reactor, the processes of combustion, pyrolysis of hydrocarbons with the formation of carbon black, occur simultaneously. The stoichiometric expression is written approximately The transformations that occur in the reactor are very complex and multi-stage, they involve a huge number of different compounds, mostly short-lived ones, many of which cannot be detected by known physical methods. Therefore, at the present, the processes under consideration cannot be fully described using the classical apparatus of chemical kinetics, and the compiled material balance is not accurate.

1.6.2 Optimization method of the solution of inverse coefficient problem

In this approach, the model of the nucleation and growth of carbon particles is also based on two ordinary differential equations that describe the instantaneous formation of the number of particles N, their mass M and having the same structure as in [9]. But the model coefficients for each source term responsible for the mechanisms of carbon nucleation and development (nucleation, coagulation, surface growth and oxidation) are determined by an optimization method for the solution of the inverse coefficient problem. The objective functions, are the values of the two specified carbon quantities obtained during natural experiment with characteristic values of the parameters of the mixture of raw materials, its evaporation products and the heat-carrier gas in the reactor. In this article, the inverse problem is formulated, and to solve it with an optimization method, a modified genetic algorithm similar to that used in [46] is constructed.

1.7 The article is organized as follows

Section 1 describes the problem statement and the approaches to solve it, as well as the assumptions that we used for the mathematical model. Section 2 contains a description of the mathematical model in FlowVision PC. That model contains continues and dispersed phases that are described by a different set of equations. In section 3 we showing the results of the numerical modeling in ANSYS PC. Several hypotheses were tested in additional to the comparison of mathematical model and experiment. Chapter 4 is devoted to substantiation of the mathematical model of the process of the carbon black particles germination and evolution. The mechanisms of being born and developing of the carbon black particles during evaporation of the oil has described in the detail. The model is being analyzed. For this model the inverse coefficient problem is posed and solved. Conclusion summarizes the study and the results are in section 5. Calculations have been carried out for the formation time change of the densities of two carbon quantities at the parameters characteristic values of the raw materials mixture, products of its evaporation and heat-carrier gas in the reactor. The found distributions of the mass and number of carbon black particles makes it possible to evaluate the dispersion and structure of the final product. An analysis was carried out for the sensitivity of the mass and number of carbon black particles to the input parameters of the constructed model.

2 The implementation of the spray atomization and evaporation of raw materials model, within the framework of the Eulerian-Eulerian approach based on the FlowVision PC

The work presents two three-dimensional Eulerian-Eulerian models of spray atomization and evaporation of raw materials injected into the chamber, created on the basis of the FlowVision PC and the ANSYS PC. The models consider a two-phase flow: the dispersed phase describes the behavior of the liquid raw material, and the carrier (gas) phase describes the mixture of natural gas combustion products and evaporated raw materials. The difference between the models lies in the approaches of describing the dispersed phase. To describe the dynamics of the dispersed phase, FlowVision PC uses convection-diffusion equations for particle concentration, momentum and phase energy. In ANSYS PC, the movement of the dispersed phase, as well as the carrier, is described by the Navier-Stokes equations. The disadvantage of the model on the FlowVision PC is the need to determine the concentration of particles at the entrance to the computational domain of the dispersed phase from the injector. Its advantage is that it is more economical than the model on the ANSYS PC.

2.1 Mathematical model

2.1.1 Motion equations

Continuity equations for the carrier phase:

$$\frac{\partial(\phi_c\rho_c)}{\partial t} + \nabla(\phi_c\rho_c\boldsymbol{V}_c) = Q_d^{\text{mass}} - M_d\dot{n}_d,$$

where ϕ_c is the volume fraction, ρ_c is the density, and $\boldsymbol{V}_c$ is the velocity of the continuous phase. Q_d^{mass} is the source term describing total evaporation (all substances evaporated mass per unit of time) from the dispersed phase. $M_d\dot{n}_d$ is the term describing the mass change of dispersed phase particles.

Momentum balance equation for the carrier phase:

$$\frac{\partial(\phi_c\rho_c\boldsymbol{V}_c)}{\partial t} + \nabla(\phi_c\rho_c\boldsymbol{V}_c\boldsymbol{V}_c) = -\phi_c\nabla p + \nabla\cdot(\phi_c\hat{\boldsymbol{\tau}}_{\text{eff}}),$$

where $\hat{\boldsymbol{\tau}}_{\text{eff}}$ is the effective viscous stress tensor, and p is the pressure. The KEFV model [65] is used to describe turbulence. The number of liquid fuel droplets per unit volume n_d is used as the main variable to describe the dynamics of the dispersed phase.

Fuel particle (dispersed phase) transport equation:

$$\frac{\partial n_d}{\partial t} + \nabla(\boldsymbol{V}_d n_d) = \nabla\left(\frac{\nu_{t,d}}{Sc_{t,d}}\nabla n_d\right) + \dot{n}_d,$$

where $\boldsymbol{V}_d$ is the dispersed phase velocity, $\nu_{t,d}$ is the turbulent kinematic viscosity coefficient of the dispersed phase (assumed to be equal to the continuous phase coefficient $\nu_{t,c}$), and $Sc_{t,d}$ is the turbulent Schmidt number for the dispersed phase (expression provided below). $\dot{n}_d$ describes particle concentration change.

Momentum balance equation for the dispersed phase:

$$\frac{\partial(\boldsymbol{V}_d M_d n_d)}{\partial t} + \nabla(M_d n_d\boldsymbol{V}_d\boldsymbol{V}_d) = \nabla\left(\frac{\nu_{t,d}}{Sc_{t,d}}\nabla(\boldsymbol{V}_d M_d n_d)\right) - n_d\frac{\pi d^3}{6}\nabla p + \boldsymbol{F}_D,$$

where $\boldsymbol{F}_D$ is the sum of external forces, and d is the Sauter mean diameter of the liquid fuel particles.

2.1.2 Equation of the mass fraction of evaporation products

The evaporated raw material is added to the heat-carrier gas, forming the carrier phase along with it. Equation for the i-th continuous phase substance mass fraction Y_i:

$$\frac{\partial(\phi_c\rho_c Y_i)}{\partial t} + \nabla(\phi_c\rho_c Y_i V) = -\nabla(\phi_c\boldsymbol{J}_{i,\text{eff}}) + Q_{d,i}^{\text{mass}}.$$

Here, $Q_{d,i}^{\text{mass}}$ is the continuous phase i-th substance mass source due to dispersed phase mass change, and $\boldsymbol{J}_{i,\text{eff}}$ is the effective diffusion flux of the i-th substance in the continuous phase:

$$\boldsymbol{J}_{i,\text{eff}} = -(\rho D_i + \mu_t/Sc_t)\nabla Y_i = -(\mu/Sc_i + \mu_t/Sc_t)\nabla Y_i,$$

where D_i is the diffusion coefficient of the i-th substance in the continuous phase, μ and μ_t are the dynamic viscosity and turbulent dynamic viscosity, respectively, and Sc_i and Sc_t are the molecular and turbulent Schmidt numbers for the i-th substance.

2.1.3 Energy Balance Equations

The energy balance equation for the continuous medium, where total enthalpy H_c is chosen as the primary variable:

$$\frac{\partial(\phi_c\rho_c H_c)}{\partial t} + \nabla(\phi_c\rho_c \boldsymbol{V}_c H_c) = \frac{\partial(\phi_c p)}{\partial t} - \nabla(\phi_c \boldsymbol{J}_q) + \phi_c Q_{\text{vis,G}} - Q_d^{\text{enth}}.$$

Here, $\boldsymbol{J}_q$ is the effective enthalpy diffusion flux, $Q_{\text{vis,G}}$ is a 'viscous' term, and Q_d^{enth} is the term describing enthalpy transfer due to evaporation.

The energy transfer for the dispersed phase:

$$\frac{\partial(h_d M_d n_d)}{\partial t} + \nabla(\boldsymbol{V}_d h_d M_d n_d) = \nabla\left(\frac{\nu_{t,d}}{Sc_{t,d}}\nabla(h_d M_d n_d)\right) + Q_d^{\text{enth}},$$

where h_d is the thermodynamic enthalpy of the particle phase, and $M_d n_d$ describes the total particle mass per unit volume at a particular point in space.

2.1.4 Fragmentation and evaporation of liquid fuel droplets

Mass transport equation of particles:

$$\frac{\partial(M_d n_d)}{\partial t} + \nabla(\boldsymbol{V}_d M_d n_d) = \nabla\left(\frac{\nu_{t,d}}{Sc_{t,d}}\nabla(M_d n_d)\right) - Q_d^{\text{mass}} + M_d \dot{n}_d.$$

This equation describes the evaporation and condensation of liquid fuel. The source term Q_d^{mass} is calculated as follows:

$$Q_d^{\text{mass}} = n_d \pi d^2 \dot{m}_d = n_d \pi d^2 \sum_{i=1}^{N_d} \dot{m}_{d,i}.$$

Here, $\dot{m}_d$ is the specific mass change rate of the particle phase, $\dot{m}_{d,i}$ is the specific mass change rate of the i-th substance of the particle phase, and N_d is the number of substances in the particle phase. Droplet fragmentation (coalescence) follows the WAVE model [66], which describes high-velocity injections in combustion chambers. The physical essence of the model is based on the development of Kelvin-Helmholtz instability on the droplet surfaces. Within the framework of this model, it is possible to calculate the diameter of liquid fuel particles, which appears in the right-hand sides of some equations.

2.2 The problem of spray atomization and evaporation of raw materials in a reactor for the furnace production of carbon black

The above model was used to solve the problem of spray atomization and evaporation of raw materials in a heat-carrier gas flow during furnace production of carbon black. In this problem, liquid raw materials (heavy hydrocarbons) is injected by six injectors, distributed uniformly along the azimuth in a plane perpendicular to the axis of the reactor, into a flow of heat-carrier gas (consisting of natural gas combustion products), as shown in Fig.3

Liquid raw materials break up into droplets and evaporate over time. After which the pyrolysis process begins to produce carbon black.

To speed up the calculation time, modeling was performed in the 60° sector of the chamber (Fig. 4) under the assumption that the solutions in other parts of the chamber are symmetrical, which introduces its own limitations: the model does not take into account gravity, in addition, the model does not allow taking into account the interaction of liquid jets when they reach the periphery of the chamber.

The geometry of the area where the system of equations described in section 2.1 is solved, as well as the boundaries where the initial-boundary conditions are set, are shown in Fig. 5. At the inlet of the carrier phase (1), its normal velocity is set to 422.69 m/s, gas temperature to

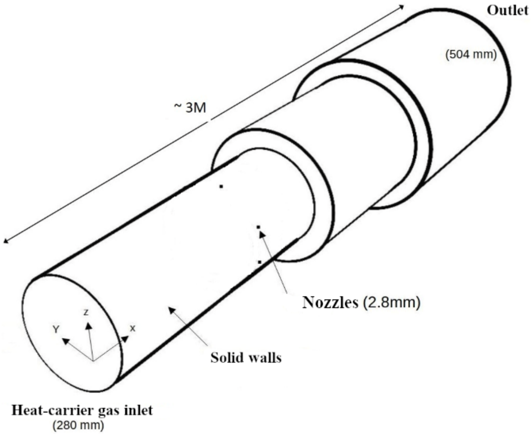

Figure 3: Reactor for the production of carbon black

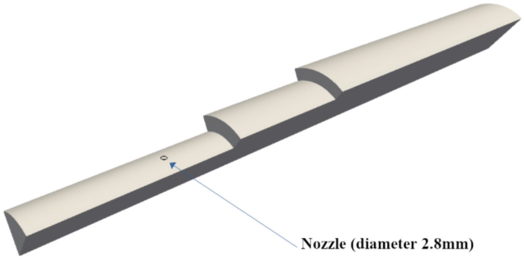

Figure 4: Reduced computational domain (sixth of the original)

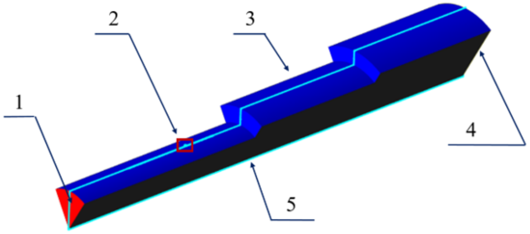

Figure 5: Boundary value conditions for the atomization and evaporation in a furnace production reactor problem. 1 – continuous phase inlet, 2 – dispersed phase inlet, 3 – wall, 4 – outlet, 5 – symmetry.

2133 K, mass fraction of substances in the carrier phase (oxygen – 0.05, carbon dioxide – 0.07, water vapor – 0.15, evaporated raw material - 0; the mass fraction of nitrogen is determined by the condition that the sum of all mass fractions equals 1), and the volume fraction of the dispersed phase is zero. At the inlet of the dispersed phase (2), its volume fraction is equal to one, the particle velocity is normal to the inlet surface and its magnitude is 27.07 m/s, and the particle phase temperature is set to 303 K. At the wall (3), the logarithmic law for the velocity of the carrier phase is set, particle collisions of the dispersed phase with the wall are considered elastic. A condition of zero temperature gradient for both phases is also set; there is no mass flow through the wall. At the outlet surface (4), the pressure is set to $1.01 \cdot 10^5$Pa. Symmetry conditions are set on the lateral surfaces of the sector (5).

Despite the fact that the described model does not include the output of carbon black, nevertheless, it allows us to obtain information about some input parameters that affect the quality of the product. For example, it is known that contact of liquid raw materials with the chamber wall leads to the appearance of coke, a by-product that contaminates carbon black. In [6], the heat-carrier gas supply rate and the diameter of the droplets at the outlet of the injector were identified as the parameters that most influence the contact of the liquid raw

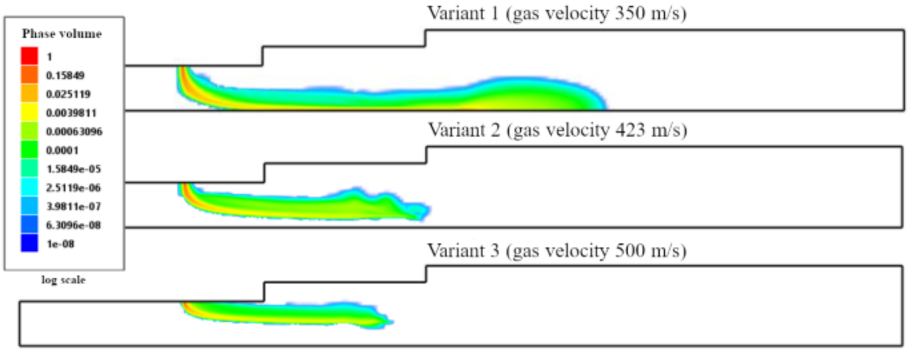

Figure 6: Distribution of the volume fraction of raw materials depending on the input velocity of the coolant gas

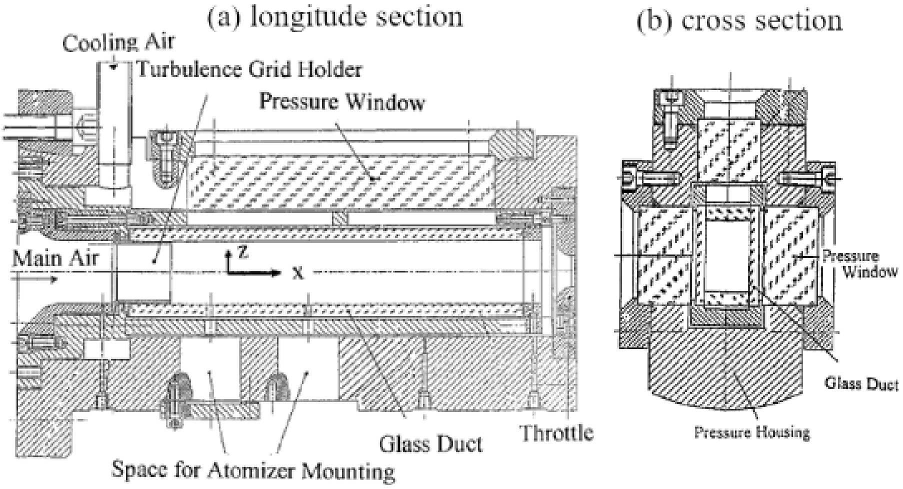

Figure 7: Experimental setup for kerosene atomization in a channel.

material with the chamber lining.

As a result of the calculations, an analysis was carried out of the sensitivity of the area of unevaporated raw materials to the heat-carrier gas supply rate. Thus, three characteristic cases for raw material spray atomization were identified. Fig. 6 shows the distribution of the volume fraction of raw materials in the reactor chamber for three heat-carrier gas velocities at the reactor inlet: 350 m/s, 423 m/s and 500 m/s. In the first case (350 m/s), a jet of liquid raw materials droplets, reaches the axis of the chamber - in this case, interaction between jets from different injectors is possible, which is not described within the framework of the given model. Droplet fragmentation occurs with low intensity; complete evaporation of raw materials is achieved only in the third section of the reactor. In the second case (426 m/s), a greater deflection of the jet along its flow and a decrease in the area of unevaporated raw material are observed. There is no contact with the reactor wall. The fragmentation of droplets becomes more intense. In the third case (500 m/s), a slight increase in the rate of droplet fragmentation and a slight decrease in the area of unevaporated raw materials are observed compared to the second mode. But at the same time, part of the raw material comes into contact with the chamber wall adjacent to the injector.

2.3 The problem of kerosene evaporation in gas turbine combustion chambers

In [67], verification of the evaporation model was presented based on a comparison between the numerical solution and an experiment on spraying kerosene, in a pre-mixing channel for

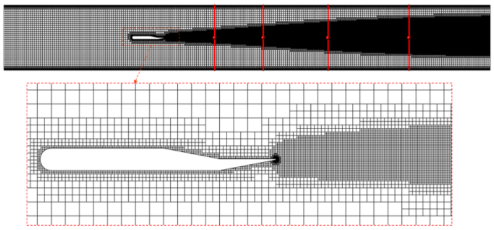

Figure 8: Computational mesh used to solve the problem

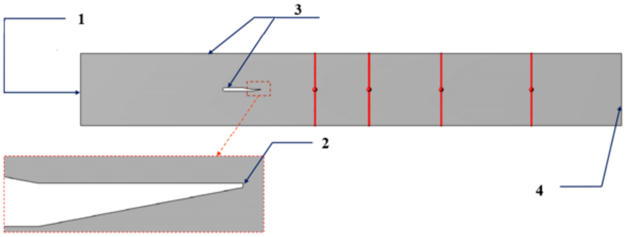

Figure 9: Boundary value conditions for the kerosene evaporation problem. 1 – continuous phase inlet, 2 – dispersed phase inlet, 3 – wall, 4 – outlet.

combustion chambers of gas turbines. The working section of the experimental setup is a rectangular channel with a cross section of 25 mm×40 mm and a flow observation area of about 180 mm (the image is given in Fig. 7). Spray atomization of the film is ensured by a high-speed flowing air. Spray width 8 mm, slot height 0.1 mm. The control sections of the computational domain, in which the flow characteristics are analyzed, are located at distances from the injector x_K=30 mm, 60 mm, 100 mm, 150 mm. The analyzed flow characteristics (hereinafter referred to as "control parameters") are taken as the fuel evaporation rate V_{evap}/V_0 (the ratio of the difference in volume flows of fuel droplets in the inlet section x_0 and control sections x_K to the flow in x_0) and the average Sauter droplet diameter SMD.

To solve this problem, the model described in Sec. 2.1 was used. The solution to the problem in a two-dimensional formulation is presented. The computational domain is shown in Fig. 8. The geometry of the area and the surfaces on which the boundary conditions were set are shown in Fig. 9. At the inlet of the carrier phase (1), the normal air mass velocity is set to 502.2575 kg/m^{2}s, temperature to 750 K, and the volume fraction of the dispersed phase to zero. At the inlet of the dispersed phase (2), the air velocity (carrier phase) is set to 106 m/s, the volume of the dispersed phase to 0.1844, as well as the fuel velocity (dispersed phase) to 10 m/s and the droplet size spectrum of the fuel particles. The air and fuel temperatures at this boundary are considered to be the same and equal to 453 K. At the wall (3), the logarithmic law for the carrier phase velocity is set, particle collisions of the dispersed phase with the wall are considered elastic, and a condition of zero temperature gradient for both phases and no mass flow through the wall is set. At the outlet (4), the pressure is set to $9{\cdot}10^5$ Pa.

As a result of the simulation, the the control parameters values of the evaporation rate of kerosene and the average Sauter diameter of kerosene droplets. Fig.10 shows a comparison between the calculated and experimental data.

The simulation results significantly depend on the size of the fuel droplets at the inlet, obtaining a correct distribution of control parameters is only possible by specifying a spectrum of droplet sizes, which allows the model to take into account changes in the acceleration of droplets by the flow, the rate of their heating and evaporation depending on the diameter; variations in the initial spectrum (selected based on the results of a cold experiment) make it possible to refine the result.

3 The Eulerian-Eulerian approach for modeling the spray atomization and evaporation with the ANSYS PC

As noted above, the most challenging stage in the process of producing carbon black in the reactor is the atomization of the raw material into the gas-heat carrier stream and its subsequent evaporation. Achieving the required degree of fineness of raw material atomization

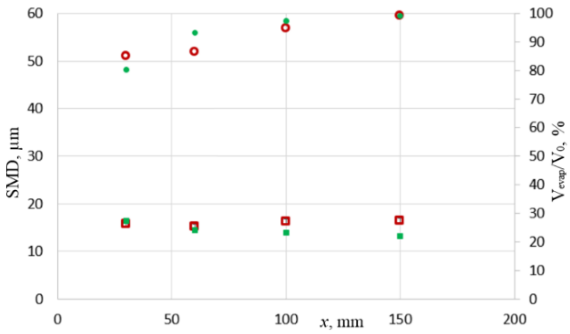

Figure 10: Values of the normalized evaporation rate (circles) and the Sauter mean diameter (squares) of fuel droplets along the x-axis. Red color – experimental values, green color – calculated values.

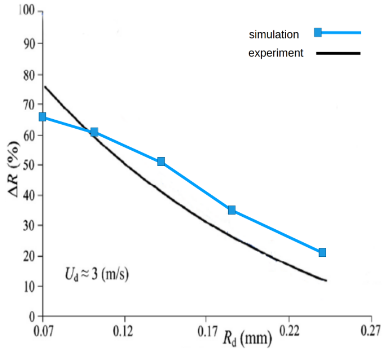

Figure 11: Comparison of evaporation degrees in the task [47], obtained experimentally (black curve) and numerically (blue curve).

and uniform droplet distribution, which would ensure its complete evaporation before pyrolysis and the necessary carbon structure, is essential. ANSYS PC offers three advanced models based on the Eulerian-Eulerian approach suitable for describing raw material atomization and evaporation. These models include the Volume of Fluid (VOF) model, the Mixture model, and the Eulerian model. To select the most accurate model for our task from these three, two test cases were solved using them. The first case involved studying the effect of droplet concentration on the evaporation rate in high-temperature gas, experimentally studied in [47]. The second case involved raw material atomization and evaporation in the reactor but was solved using another numerical model [6]. A two-phase model was used to solve these tasks. One phase-the carrier phase-consisted of a mixture of gas-heat carrier and evaporation products of the liquid. The second phase-the dispersed phase-consisted of water in the first task and liquid hydrocarbons in the second task. Comparing the evaporation rates obtained numerically using the Lee evaporation model in any of the three multiphase models mentioned and experimentally [47], showed the unsuitability of the Lee model for arbitrary cases. This is due to the need for time relaxation parameter calibration in the model, which requires experimental data. The Raoul evaporation model was also investigated. Its drawback is the ANSYS PC package's requirement to use this model only in conjunction with the Eulerian or Mixture models, but not with VOF. Therefore, after thorough testing of the VOF, Mixture, and Eulerian models with the Lee and Raoul evaporation models on the specified test tasks, the Eulerian model with the Raoul evaporation model was chosen for further research. The equations of this model are presented below.

3.1 Mathematical model

3.1.1 Motion equations

The continuity equation for the carrier phase is expressed as:

$$\frac{\partial\left(\alpha_c \rho_c\right)}{\partial t}+\nabla\left(\alpha_c \rho_c \boldsymbol{u}_c\right)=\dot{m}_{lc}-\dot{m}_{cl}.$$

Where α_c represents the volume fraction of the carrier phase, $\boldsymbol{u}_c$ denotes the velocity of the carrier phase, ρ_c is the density of the carrier phase, $\dot{m}_{lc}$ is the mass transfer from the liquid phase to the carrier phase, and $\dot{m}_{cl}$ is the mass transfer from the carrier phase to the liquid phase.

The volume fraction of the dispersed phase α_l is calculated using the formula:

$$\alpha_l = 1 - \alpha_c.$$

In the Eulerian model, each phase has its own momentum conservation equation, but with the same pressure for both phases

$$\begin{aligned}\frac{\partial\left(\alpha_c\rho_c\boldsymbol{u}_c\right)}{\partial t}&+\nabla\left(\alpha_c\rho_c\boldsymbol{u}_c\boldsymbol{u}_c\right)=\\&-\alpha_c\nabla p+\nabla\left(\alpha_c\widehat{\boldsymbol{\tau}}_{eff,c}\right)+\alpha_c\rho_c\boldsymbol{g}+K\left(\boldsymbol{u}_c-\boldsymbol{u}_l\right)+\dot{m}_{lc}\boldsymbol{u}_{lc}-\dot{m}_{cl}\boldsymbol{u}_{cl},\end{aligned}\tag{4}$$

$$\begin{aligned}\frac{\partial\left(\alpha_l\rho_l\boldsymbol{u}_l\right)}{\partial t}&+\nabla\left(\alpha_l\rho_l\boldsymbol{u}_l\boldsymbol{u}_l\right)=\\&-\alpha_l\nabla p+\nabla\left(\alpha_l\widehat{\boldsymbol{\tau}}_{eff,l}\right)+\alpha_l\rho_l\boldsymbol{g}+K\left(\boldsymbol{u}_l-\boldsymbol{u}_c\right)+\dot{m}_{cl}\boldsymbol{u}_{cl}-\dot{m}_{lc}\boldsymbol{u}_{lc}.\end{aligned}\tag{5}$$

In this context, p denotes the same pressure across all phases, $\boldsymbol{g}$ signifies gravity, and K is the coefficient for interphase momentum exchange. The effective stress tensor for the carrier phase is $\widehat{\boldsymbol{\tau}}_{eff,c}$, while for the liquid phase, it is $\widehat{\boldsymbol{\tau}}_{eff,l}$. The liquid's density is represented by ρ_l, and its velocity by $\boldsymbol{u}_l$. The interfacial velocities, $\boldsymbol{u}_{cl}$ and $\boldsymbol{u}_{lc}$, are defined as follows: if $\boldsymbol{u}_{lc}>0$, indicating mass transfer from the liquid phase to the carrier phase, then $\boldsymbol{u}_{lc}=\boldsymbol{u}_l$; if $\boldsymbol{u}_{lc}<0$, indicating mass transfer from the carrier phase to the liquid phase, then $\boldsymbol{u}_{lc}=\boldsymbol{u}_c$.

The terms $\hat{\boldsymbol{\tau}}_{eff,c}$, $\hat{\boldsymbol{\tau}}_{eff,l}$ are defined as follows:

$$\hat{\boldsymbol{\tau}}_{eff,c}=\mu_{eff,c}(\nabla\boldsymbol{u}_c+\nabla\boldsymbol{u}_c^T)+\frac{2}{3}(\rho_c k-\mu_{eff,c}\nabla\boldsymbol{u}_c)\hat{\boldsymbol{I}},\quad \mu_{eff,c}=\mu_t+\mu_c,$$

$$\hat{\boldsymbol{\tau}}_{eff,l}=\mu_{eff,l}(\nabla\boldsymbol{u}_l+\nabla\boldsymbol{u}_l^T)+\frac{2}{3}(\rho_l k-\mu_{eff,l}\nabla\boldsymbol{u}_l)\hat{\boldsymbol{I}},\quad \mu_{eff,l}=\mu_t+\mu_l.$$

μ_t – turbulent viscosity, μ_c – viscosity of the carrier phase, μ_l – viscosity of the liquid phase, k – kinetic turbulent energy.

3.1.2 Mass fraction equation of liquid evaporation products

Monitoring of liquid evaporation products is done using the variable Y_v, which represents the mass fraction of these products. This variable adheres to the convection-diffusion equation:

$$\frac{\partial\left(\alpha_c\rho_c Y_v\right)}{\partial t}+\nabla\cdot\left(\alpha_c\rho_c\boldsymbol{u}_c Y_v\right)=-\nabla\cdot\left(\alpha_c\boldsymbol{J}_v\right)+\dot{m}_{lc}-\dot{m}_{cl}.$$

Here, $\boldsymbol{J}_v$ refers to the diffusive flow of liquid evaporation products and is expressed as:

$$\boldsymbol{J}_v=-\left(\rho_c D_{v,c}+\frac{\mu_t}{Sc_t}\right)\nabla Y_v,$$

where $D_{v,c}$ is the mass diffusion coefficient of the liquid evaporation products, Sc_t represents the turbulent Schmidt number, and μ_t is the turbulent viscosity. The density of the carrier phase, ρ_c, is computed using the densities of the liquid evaporation products ρ_v and the heat-carrier gas ρ_g as follows:

$$\rho_c=Y_v\rho_v+\left(1-Y_v\right)\rho_g.$$

3.1.3 Energy conservation equations

In the Eulerian model, each phase has its own energy conservation equation

$$\begin{aligned}\frac{\partial(\alpha_c\rho_c h_c)}{\partial t}&+\nabla(\alpha_c\rho_c\boldsymbol{u}_c)=\\&\alpha_c\frac{\partial p}{\partial t}+[\alpha_c\widehat{\boldsymbol{\tau}}_{eff,c}]\nabla\boldsymbol{u}_c-\nabla(\alpha_c\kappa_{eff,c}\nabla T_c)+Q_{lc}+\dot{m}_{lc}h_{lc}-\dot{m}_{cl}h_{cl},\end{aligned}\tag{6}$$

$$\begin{aligned}\frac{\partial(\alpha_l\rho_l h_l)}{\partial t}&+\nabla(\alpha_l\rho_l\boldsymbol{u}_l)=\\&\alpha_l\frac{\partial p}{\partial t}+[\alpha_l\widehat{\boldsymbol{\tau}}_{eff,l}]\nabla\boldsymbol{u}_l-\nabla(\alpha_l\kappa_{eff,l}\nabla T_l)+Q_{cl}+\dot{m}_{cl}h_{cl}-\dot{m}_{lc}h_{lc}.\end{aligned}\tag{7}$$

Here, h_c is the sensible enthalpy of the carrier phase, $\kappa_{eff,c}$ is the effective thermal conductivity of the carrier phase, T_c is the temperature of the carrier phase, h_l is the sensible enthalpy of the dispersed phase, $\kappa_{eff,l}$ is the effective thermal conductivity of the dispersed phase, T_l is the temperature of the dispersed phase, $Q_{lc} = -Q_{cl}$ represents the heat transfer between the phases, and h_{cl} and h_{lc} are the interfacial enthalpies.

The terms h_c, h_{cl}, $\kappa_{eff,c}$, $\kappa_{eff,l}$ are defined as follows:

$$h_c = c_{p,c}(T_c - T_{ref}), \quad h_l = c_{p,l}(T_l - T_{ref}), \quad \kappa_{eff,c} = \kappa_c + \frac{c_{p,c}\mu_t}{Pr_t}, \quad \kappa_{eff,l} = \kappa_l + \frac{c_{p,l}\mu_t}{Pr_t}.$$

Here, κ_c, κ_l are the thermal conductivities of the carrier and liquid phases, T_{ref} is the reference temperature, $c_{p,c}$, $c_{p,l}$ are the heat capacities of the carrier and liquid phases, Pr_t is the turbulent Prandtl number.

3.1.4 The interphase momentum exchange coefficient

The equations (4) and (5) includes the interphase momentum exchange coefficient. The formula for this coefficient is derived from the assumption that "the dispersed phase consists of droplets" and has the following general form $K = \rho_l f d_l A/(6\tau_l)$. Here A is the interfacial surface, d_l is the droplets diameter of the dispersed phase, f is the resistance function, τ_l is the particles relaxation time, which is determined as follows $\tau_l = \rho_l d_l^2/(18\mu_c)$. The resistance function is determined with the Schiller and Naumann formula [48] $f = C_d\mathrm{Re}/24$, where $C_D = 24(1+0.15\mathrm{Re}^{0.687})/\mathrm{Re}$ if $\mathrm{Re} \leq 1000$, and $C_D = 0.44$ if $\mathrm{Re} > 100$. Re is relative Reynolds number: $\mathrm{Re} = \rho_c|u_c - u_l|d_l/\mu_c$. The interfacial surface is defined as follows: $A = 6/d_l$.

3.1.5 Heat transfer coefficient

The Eqs. (6) and (7) includes the heat transfer coefficient. This coefficient is assumed to be a function of the temperature difference and the interfacial surface. $Q_{lc} = \kappa_c \mathrm{Nu}_l A(T_l - T_c)/d_l$. Here Nu_l is the Nusselt number of the liquid phase, modeled using the Rantz-Marshall model [49,50] $\mathrm{Nu}_l = 2+0.6\mathrm{Re}^{0.5}\mathrm{Pr}^{1/3}$. Here Pr is the Prandtl number of the carrier phase, determined as follows: $\mathrm{Pr} = c_{p,c}\mu_c/\kappa_c$.

3.1.6 Mass transfer

ANSYS PC, it is provided several ways to model the evaporation process. The most common and simple is the Lee evaporation model [51]. One of the requirements of this model is to set the parameters of time relaxation. These parameters are found by calibrating experimental data. In another evaporation model, mass transfer occurs across the phase boundary with a volumetric velocity that depends on the gradient of the mass concentration of the transferred particles in different phases. $\dot{m}_{lc} = k_{lc}A(K_{vl}^{\rho}\rho_l - \rho_v)$. Here, k_{lv} represents the volumetric mass transfer coefficient between the dispersed phase and its vapors, while k_{vl}^{ρ} denotes the equilibrium ratio. Parameters k_{lv} and k_{vl}^{ρ} are calculated using the law of two resistances, first proposed by Whitman [52] $1/k_{lv} = 1/k_v + K_{vl}^{\rho}/k_l$.

Here, k_l represents the liquid mass transfer coefficient, while k_v denotes the mass transfer coefficient of the liquid evaporation products. Equilibrium relationship (k_{vl}^{ρ}) according to Raoult's formula $K_{vl}^{\rho} = P/P_{sat}^{v}$. Here P_{sat}^{v} is the saturation temperature of liquid evaporation products.

3.2 The effect of droplet concentration on evaporation rates in high-temperature gas environments

In [47], the effect of water droplet concentration on their degree of evaporation was experimentally studied when injecting a mixture of water droplets and air into a cylinder filled with gas at a temperature of $T = 1070K$. The cylinder has a diameter of 0.15 m and a length of 1

m. The initial temperature of the water droplets before mixing into the cylinder is $T = 300K$. The initial size of the water droplets impacts their evaporation degree, and [47] determines the relationship between the concentration of water droplets in the mixture and their evaporation degree. The evaporation degree ΔR in [47] is calculated using the following formula: $\Delta R = \left(R_d - R_d^*\right)/R_d \cdot 100\%$. At the cylinder's inlet section, the average droplet size is kept constant at R_d, the volume ratio of water to air in the sprayed mixture is taken as $\gamma_{\text{in}} = 10^{-3}$, the water droplet velocity is set to $|u_d| = 3$ m/s, and the air velocity is $|u_a| = 1.5$ m/s. The droplet size at the cylinder's outlet section is denoted as R_d^*.

In the calculations, the evaporation degree ΔF is found by the formula $\Delta F = (F_{\text{in}} - F_{\text{out}})/F_{\text{in}} \cdot 100\%$, where F_{in} is the mass flow rate of water at the cylinder's inlet section and F_{out} is the mass flow rate of water at the cylinder's outlet section. In the calculations, the droplet size of the liquid phase at the inlet section is d_l.

At the inlet section, the liquid phase velocity is set to $|u_l| = 3$ m/s and its temperature $T_l = 300K$. For the carrier phase, the velocity is $|u_c| = 1.5$ m/s, temperature $T_c = 1070K$, and mass fraction of evaporation products $Y_v = 0$. The volume fraction of the liquid α_l is calculated from γ_{in} as follows:

$$\alpha_l = \frac{V_w}{V_w + V_a} = \frac{V_w}{V_g\left(\frac{V_w}{V_g} + 1\right)} = \frac{V_w/V_g}{1 + V_w/V_g} = \frac{\gamma_{\text{in}}}{1 + \gamma_{\text{in}}}.$$

Here, V_w and V_g are the volumes of water and gas. The volume fraction of the carrier phase $\alpha_c = 1 - \alpha_l$. On the solid wall, the no-slip condition is used. At the outlet, the pressure is fixed at 1 atm. The physical properties of water and air are set by default in the ANSYS PC database. The evaporation degrees ΔF were calculated for five values of d_l (0.07 mm, 0.1 mm, 0.145 mm, 0.19 mm, and 0.245 mm). In Fig. 11, the dependence $(d_l, \Delta F)$ is shown with blue lines and rectangles, where the rectangles represent the results of numerical modeling with given d_l values. The dependence $(R_d, \Delta R)$ is shown in black. The dependence $(d_l, \Delta F)$ corresponds to the expected behavior: the smaller the droplet size, the higher the evaporation degree. The maximum difference in evaporation degree between the numerically obtained curve $(d_l, \Delta F)$ and experimentally found $(R_d, \Delta R)$ is less than 10%, confirming the good resolution capability of the used model in solving mass transfer problems.

3.3 Atomization and evaporation of raw materials in a reactor for furnace carbon black production

Liquid hydrocarbon is injected at a velocity of 27 m/s and a temperature of 30Γ,°C from six injectors, which are uniformly distributed around the circumference of the reactor's cross-section. This is done into a heat-carrier gas flow (natural air combustion products) supplied at a velocity of 422 m/s and a temperature of 1860Γ,°C (Fig. 3). Liquid raw materials break up into droplets and evaporate over time. After which the pyrolysis process begins to produce carbon black. In [5] another model was used to solve this problem, and the evaporation degree was calculated for droplets with a diameter of 1.4 mm. To reduce the computation time, this problem was solved in a section (one-sixth of the circumferential direction of the original computational domain) in which there is only one injector (Fig. 4).

Our model was used to solve this problem as well, and a comparison was conducted. The evaporation degree is calculated the same way as in the previous problem for d_l=1.4 mm. The boundary conditions for the described model are given as following: at the heat-carrier gas inlet: $|\boldsymbol{u}_c|$= 422 m/s, T_c=1860°C, α_c=1, Y_v=0, $|\boldsymbol{u}_l|$=0 m/s, T_l=30°C, α_l=0; on the injector: $|\boldsymbol{u}_c|$=0 m/s, T_c=1860°C, α_c=0, Y_v=0, $|\boldsymbol{u}_l|$=27 m/s (perpendicular to the boundary), T_l=30°C, α_l=1; on the side boundariesm the symmetrical conditions are used; non-slip conditions for

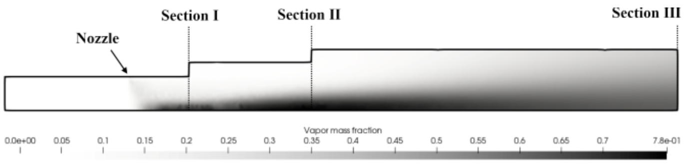

Figure 12: Mass fraction of evaporation products of liquid raw materials in the longitudinal section.

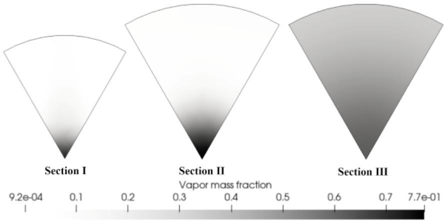

Figure 13: Mass fraction of evaporation products of liquid raw materials in cross sections.

the solid wall; at the outlet, the pressure is fixed at 1 atm. The physical properties of the materials specified as in [5].

Based on the results obtained from the presented model, the mass fraction of evaporation products of liquid raw materials Y_v can be seen in various sections (Fig. 12 and Fig. 13). The flow rate of liquid raw materials at the injector is 0.166 kg/s, while the flow rate of the carrier phase at its inlet is 0.617 kg/s. At the reactor outlet, the flow rate of liquid raw materials is 0.063 kg/s, and the flow rate of the carrier phase is 0.720 kg/s. Comparing the flow rates of the liquid raw materials at the injector and the outlet, we observe a decrease of $0.063 - 0.166 = -0.103$ kg/s. Comparing the flow rates of the carrier phase at it's inlet and outlet, we observe an increase of $0.720 - 0.617 = +0.103$ kg/s. This indicates that evaporation is indeed taking place. The decrease in the flow rate of liquid raw materials is equal in magnitude to the increase in the flow rate of the carrier phase, demonstrating that the conservation of mass for the raw material in both liquid and gaseous forms is maintained. The evaporation degree is described as a percentage of reduction in the flow rate of liquid raw materials $(0.063 - 0.166)/0.166 \approx 62\%$, this degree is very close to that obtained in [5] (64%). Overall the results are considered very good: comparison difference is 2%.

3.4 Results discussion

In the problem of the influence of droplet concentration on the evaporation degree in a high-temperature gas, a relationship was established between the droplet size d_l: 0.07 mm, 0.1 mm, 0.145 mm, 0.19 mm and 0.245 mm and evaporation degree ΔF. The dependence $(d_l,\Delta F)$ shows the expected behavior: the smaller the droplet size, the greater the degree of evaporation. Comparing the dependence $(d_l, \Delta F)$ with $(R_d,\Delta R)$ – the corresponding dependence of the experimental data, shows a fairly good match, with a maximum difference of up to 10%. Overall the results are considered quite good.

In addressing the atomization and evaporation of raw materials in a furnace reactor for carbon black production, it was observed that the decrease in the flow rate of liquid raw materials matches the increase in the flow rate of the carrier phase. This indicates that the conservation of mass for the raw materials in both liquid and gaseous forms is maintained. A comparison of the degrees of evaporation of the presented model and the model [5] shows a very good agreement (the difference is 2%).

4 Carbon black formation model

4.1 Moss-Brookes model of the nucleation and growth of carbon particles

We will take the Moss-Brookes model presented in [53] as the basis for the model of carbon black formation in the reactor. It consists of two equations that describe the behavior of the density of the carbon black particles number $N[\mathrm{m}^{-3}]$ and the mass density of carbon black $M[\mathrm{kg/m}^3]$, with time

$$\begin{aligned}
\frac{dN}{dt} &= \alpha - \beta M^{1/6} N^{11/6}, && (8)\\
\frac{dM}{dt} &= \alpha_1 + (\gamma - \delta)\, M^{2/3} N^{1/3}. && (9)
\end{aligned}$$

At the initial time, both quantities are absent in the evaporation products of liquid hydrocarbons: $N(0) = 0$, $M(0) = 0$.

Model coefficients are calculated using the formulas:

$$\begin{aligned}
\alpha &= c_1 N_A \left(\rho \frac{Y_{C_2H_2}}{W_{C_2H_2}}\right) \exp\left\{-\frac{21100}{T}\right\}, && (10)\\
\alpha_1 &= \alpha \frac{M_p}{N_A}, && (11)\\
\beta &= \left(\frac{24R}{\rho_{soot} N_A}\right)^{1/2} \left(\frac{6}{\pi \rho_{soot}}\right)^{1/6} T^{1/2}, && (12)\\
\gamma &= c_4 \left(\rho \frac{Y_{C_2H_2}}{W_{C_2H_2}}\right) \pi^{1/3} \left(\frac{6}{\rho_{soot}}\right)^{2/3} \exp\left\{-\frac{12100}{T}\right\}, && (13)\\
\delta &= c_5 \eta \rho \frac{Y_{OH}}{W_{OH}} \pi \left(\frac{6}{\rho_{soot}}\right)^{2/3} T^{1/2} - c_6 \rho \frac{Y_{O_2}}{W_{O_2}} \pi^{1/3} \left(\frac{6}{\rho_{soot}}\right)^{2/3} T^{1/2} \exp\left\{-\frac{19778}{T}\right\}. && (14)
\end{aligned}$$

The model coefficients depend on the following five parameters of the gas in which soot nucleates: ρ – density of the gas mixture in which soot is formed, $Y_{C_2H_2}$ – mass fraction of acetylene, Y_{OH} – mass fraction of OH radical, Y_{O_2} – mass fraction of oxygen, T – temperature of the gas mixture.

The remaining model constants are given in Tab. 2.

Table 2: Model constants of the problem, their dimensions and values.

Constant	Name	unit	Value
c_1			54
c_4		kg· m· kmol^{-1}· s^{-1}	9000.6
c_5		kg· m· kmol^{-1}· K$^{\frac{-1}{2}}$ · s^{-1}	105.81
c_6		kg· m· kmol^{-1}· K$^{\frac{-1}{2}}$ · s^{-1}	8903.51
η	Collision efficiency parameter		0.13
R	Gas constant	J· mol^{-1}· K^{-1}	8.31
M_p	Molar mass of soot particle	kg· kmol^{-1}	1200
N_A	Avogadro's constant	kmol^{-1}	6.02×10^{26}
$W_{C_2H_2}$	Molar mass of acetylene	kg· kmol^{-1}	26
W_{OH}	Molar mass of radical OH	kg· kmol^{-1}	17
W_{O_2}	Molar mass of radical O_2	kg· kmol−1	32
ρ_{soot}	Soot density O_2	kg· m^{-13}	2000

In [53], it was presented the distributions of parameters $Y_{C_2H_2}$, Y_{OH}, Y_{O_2}, T, calculated within a certain model of the aromatic hydrocarbons formation in the reaction mixture. These distributions make it possible to estimate the value limits, within which these parameters vary. The values of the limits of the ranges of parameter changes are given in Tab. 4.2. There are no density distributions for the gas mixture in [53]. However, in [54] (the problem statement for [53]), the mass flow rate, velocity and area of the injector from which the gas flows are given. According to these data, the density value at the entrance to the computational domain is about 0.84 kg/m^3. Assuming compression of the mixture by 10 times in one direction or another, we obtain an estimate for the density range (see Tab. 3).

Table 3: Ranges limits for changing gas parameters.

Parameter	Range of change
ρ,kg$\cdot$ m^{-3}	0.085 - 8.4
$Y_{C_2H_2}$	$4.0 \times 10^{-3} - 2.1 \times 10^{-2}$
Y_{OH}	$5.8 \times 10^{-4} - 1.2 \times 10^{-3}$
Y_{O_2}	$3.9 \times 10^{-2} - 1.2 \times 10^{-1}$
Y,T	$500 - 1600$

4.2 The theoretical basis of the Moss-Brooks model

Brooks and Moss [55] use soot particle number N and mass density M to describe the uniform and instantaneous uncontrolled formation and development of carbon during combustion of acetylene. We assume that the behavior of technical carbon during its furnace production is similar.

4.2.1 Moss-Brooks model

The equations structure of Moss-Brooks model can be presented as following:

$$\frac{dN}{dt} = A - B, \tag{15}$$

$$\frac{dM}{dt} = C + D - E, \tag{16}$$

where the source terms in right sides of the equations are substituted by there formulas. For the soot nucleation [53] answers:

$$A = c_1 N_A \left(\rho \frac{Y_{C_2H_2}}{W_{C_2H_2}}\right) \exp\left\{-\frac{21100}{T}\right\}, \quad B = \left(\frac{24R}{\rho_{soot} N_A}\right)^{1/2} \left(\frac{6}{\pi \rho_{soot}}\right)^{1/6} T^{1/2} M^{1/6} N^{11/6}.$$

For the soot coagulation [56]:

$$C = c_1 N_A \left(\rho \frac{Y_{C_2H_2}}{W_{C_2H_2}}\right) \exp\left\{-\frac{21100}{T}\right\} \frac{M_p}{N_A}.$$

For the soot growth [57-59]:

$$D = c_4 \left(\rho \frac{Y_{C_2H_2}}{W_{C_2H_2}}\right) (\pi N)^{1/3} \left(\frac{6M}{\rho_{soot}}\right)^{2/3} \exp\left\{-\frac{12100}{T}\right\}.$$

For the soot oxidation [60-62]:

$$E = -\rho (\pi N)^{1/3} \left(\frac{6M}{\rho_{soot}}\right)^{2/3} T^{\frac{1}{2}} \left(c_5 \eta \frac{Y_{OH}}{W_{OH}} + c_6 \frac{Y_{O_2}}{W_{O_2}} \exp\left\{-\frac{19778}{T}\right\}\right).$$

Eqs. (15) and (16) are a compact form of Eqs. (8) and (9).

4.2.2 The relationship between carbon kinetics and the dynamics of the carrier phase flow field

The process of carbon formation is highly dependent on temperature and carrier phase dynamics. Therefore, it is advisable to connect two concipts together. The continuty equation of carrier phase:

$$\frac{\partial}{\partial t}\rho_c + \nabla(\rho_c \boldsymbol{u}_c) = R_{P,m},$$

The momentume balance equation:

$$\frac{\partial}{\partial t}(\rho_c \boldsymbol{u}_c) + \nabla(\rho_c \boldsymbol{u}_c \boldsymbol{u}_c) = -\nabla p + \nabla \boldsymbol{\tau}_{eff} + \rho_c \boldsymbol{g} + R_{P,mom}.$$

The energy balance equation:

$$\frac{\partial}{\partial t}(\rho_c E) + \nabla\left(\boldsymbol{u}_c(\rho_c E + p)\right) = \nabla\left(a_{eff}\nabla h_{sen}\right) + R_h + R_{P,h} + R_{rad}.$$

The equation of component m:

$$\frac{\partial}{\partial t}(\rho_c Y_m) + \nabla(\rho_c \boldsymbol{u}_c Y_m) = \nabla\left(\rho_c D_{eff}\nabla Y_m\right) + R_{P,Y_m} + R_{Y_m}.$$

The equation of carbon formation:

$$\frac{\partial}{\partial t}(\rho_c Y_{soot}) + \nabla(\rho_c \boldsymbol{u}_c Y_{soot}) = \nabla\left(D_{eff}\nabla Y_{soot}\right) + \frac{dM}{dt}.$$

$$\frac{\partial}{\partial t}(\rho_c N) + \nabla(\rho_c \boldsymbol{u}_c N) = \nabla\left(D_{eff}\nabla N\right) + \frac{dN}{dt}.$$

In here, Y_m – the mass fraction of carrier phase component m, Y_{soot} – the mass fraction of carbon, R_h – reaction enthalpy, $R_{P,m}$ – mass source term from particle, $R_{P,h}$ – enthalpy source term from particle, R_{rad} – energy source term of radiation, R_{P,Y_m} – species source term from particle, R_{Y_m} – species source term from reactions, $R_{P,mom}$ – momentum source term.

4.3 Numerical method

System of equations (8)-(9) is written in vector form

$$\frac{d\boldsymbol{X}}{dt} = \boldsymbol{F}(t, \boldsymbol{X}), \qquad \boldsymbol{X} = \begin{pmatrix} N \\ M \end{pmatrix}, \quad \boldsymbol{F} = \begin{pmatrix} \alpha - \beta M^{1/6} N^{11/6} \\ \alpha_1 + (\gamma - \delta) M^{2/3} N^{1/3} \end{pmatrix}. \tag{17}$$

and is solved numerically by the 2nd order Runge-Kutta method [68]

$$\boldsymbol{X}^{n+1} = \boldsymbol{X}^n + \tau \boldsymbol{F}\left(t^n + \frac{\tau}{2}, \boldsymbol{X}^n + \frac{\tau}{2}\boldsymbol{F}(t^n, \boldsymbol{X}^n)\right), \tag{18}$$

where τ is the time step, n is the number of the partition point of the time interval $[0, T_t]$.

4.4 The numerical solution of the Moss-Brookes model for the nucleation and growth of carbon particles and its analysis

In order to identify the peculiarities of the behavior of the Moss-Brookes model solution over a sufficiently large time interval from the point of view of the solution reaching a stationary regime, the time dependences of N and M were numerically obtained by varying the gas parameters in which soot nucleated (Figs. 14-17).

Based on the obtained solution patterns, the following conclusions can be drawn. The carbon concentration N behaves generally linearly, which is due to the significant influence of the formation component α. In this case, the following can be highlighted: at a high temperature of the mixture of fuel combustion products, the solution relatively quickly becomes constant in time. This is because of inhibition, due to the factors of coagulation, growth and oxidation, which probably occur more actively at high temperatures of the gas mixture. This effect can also be seen in the graphs in which the transition to a stationary state was not observed. When viewed on logarithmic axes, one can notice a decrease in growth tempo, which is probably due to the same factors. As for mass density, the solution patterns, as one would expect, are different when varying the parameters of the problem, but it is easy to see that the solution has a common structure: a sharp jump at the beginning, balanced by the growth and oxidation coefficients, which subsequently ensure a decrease in mass density. In some of the obtained solutions, in which the decrease occurred at a fairly sharp rate, a subtle jump in the growth of mass density was observed at the moment when the latter reaches such a low value that the partition and the condition $M > 0$ allows. When considering the mathematical model, it possible to see that at $M << 1$ the influence of the coagulation, growth and oxidation coefficients is reduced, thereby we are actually observing linear growth, which, after some time, will be smoothed out due to the above coefficients. It is logical to assume that some cyclicity will be observed. It is difficult to determine the nature of this phenomenon, however, if we take into account that the model was compiled with significant simplifications both at the stage of the physical modeling (for example, we did not take into account the reactions occurring between the supplied raw materials and hydrocarbons in the combustion products) and at the stage of the mathematical modeling, it can be assumed that such behavior is a feature of the mathematical model.

4.5 One of the possible approaches to generalizing the Moss-Brookes model of carbon formation in an acetylene combustion flame to the case of carbon black formation in a reactor in a mixture of raw materials and its evaporation products

The Moss-Brookes model under consideration describes the process of soot formation in the flame of combustion products. Taking into account the accepted simplification of direct pyrolysis of carbon from acetylene $C_2H_2 \to 2C + H_2$, the following parameters are highlighted in the physical model: ρ – the density of the gas mixture of fuel combustion products, $Y_{C_2H_2}$, Y_{OH}, Y_{O_2} – mass fractions of acetylene, hydroxyl radicals and oxygen in the gas mixture formed in the combustion flame, T – temperature of the flame.

This model can be promisingly generalized to the case of carbon black formation during the furnace process. However, there are obvious differences, since the formation occurs as a result of the interaction of active raw materials; in a simplified way, we are considering the

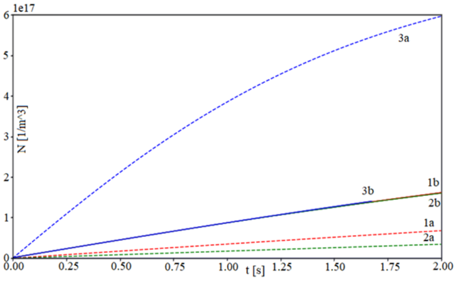

Figure 14: Dependencies of the number of soot particles N on time t in the interval $[0, 2]$ for different values of the model coefficient α: 1a) 8.83×10^{16}; 2a) 1.76×10^{17}; 3a) 4.41×10^{17}; and δ: 1b) 8.24×10^{-4}; 2b) 4.12×10^{-3}; 3b) 1.64×10^{-4}.

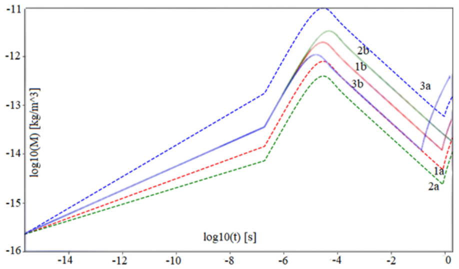

Figure 15: Dependencies of the mass of soot particles M on time t in the interval $[0, 2]$ for different values of the model coefficient α: 1a) 8.83×10^{16}; 2a) 1.76×10^{17}; 3a) 4.41×10^{17}; and δ: 1b) 8.24×10^{-4}; 2b) 4.12×10^{-3}; 3b) 1.64×10^{-4}.

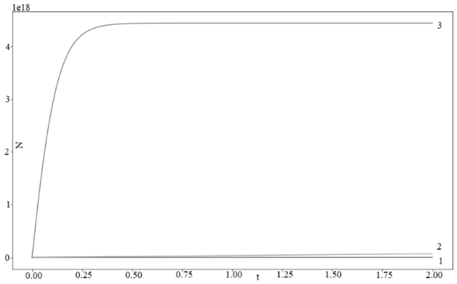

Figure 16: Dependencies of soot particles number N on t in the interval $[0, 2]$ for different values of temperature T: 1) 500 K; 2) 1050 K; 3) 1600 K.

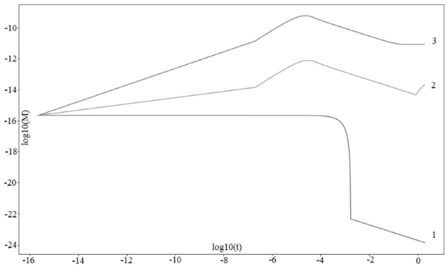

Figure 17: Dependencies of soot particles mass M on time t in the interval $[0, 2]$ for different values of temperature T: 1) 500 K; 2) 1050 K; 3) 1600 K.

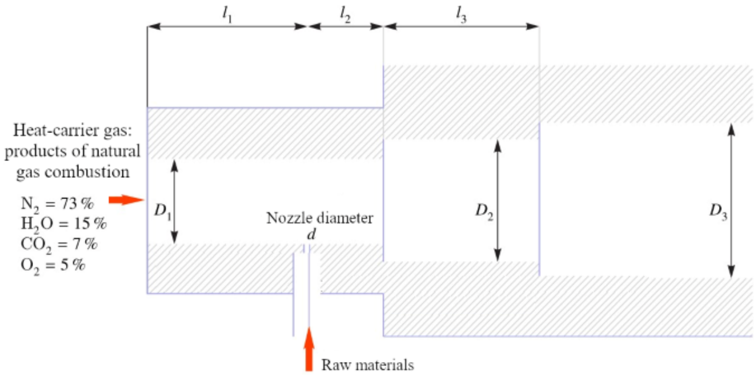

Figure 18: Approximate model of a reactor for the furnace process of carbon black production

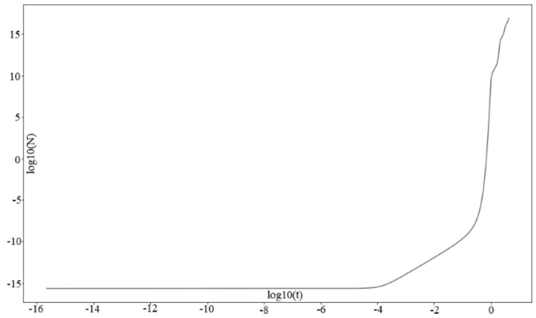

Figure 19: Dependence of soot particles number N on time t over an interval $(0, 4.25)$ in logarithmic scale during the furnace process of carbon black production.

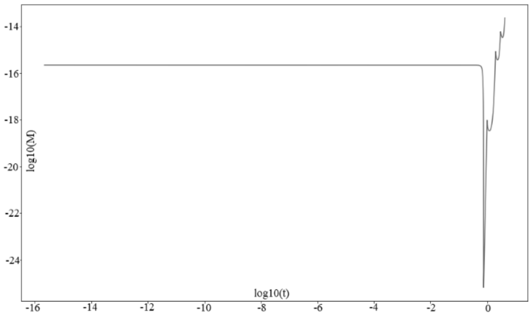

Figure 20: Dependence of soot particles mass M on time t over an interval $(0, 4.25)$ in logarithmic scale during the furnace process of carbon black production.

same acetylene, and fuel combustion products. Under this condition, the following can be said about the modifications of the physical model parameters.

Starting with density, it's obviously undergoes a significant changes, mainly associated with a much larger area of distribution for the gas mixture and the reactor design (furnace), which separately supplies raw materials and fuel combustion products, unlike in a combustion flame, the density, due to the small volume distribution, can be estimated by some constant throughout the entire volume. The medium formed in the reactor is extremely heterogeneous; the content cannot be assessed only by the parameters of the injector. Several options can be considered, for generalizing the soot formation model to the case that interest us. Firstly, the density can still be averaged over the entire reactor, and obviously, if the reagents are supplied constantly, then it is not fixed in time. However, knowing the intensity of raw material supply and fuel combustion, the corresponding calculations are not difficult to carry out. Secondly, the region can be divided into small subregions in which the parameter can be considered constant. The advantage is, the greater plausibility with reality, due to fewer simplifications. The downside is that calculations are carried out separately for each subarea, which means it takes longer time; the result obtained can only be verified based on the final output, since in practice, calculating the output in each subarea is practically impossible.

Similar reasoning can be applied to other parameters. It is worth noting some difficulties when calculating mass fractions. In the first case, the problem, after averaging the results over the entire volume, differs little from the original problem (the combustion in flame), in the second, we obviously will not be able to follow the distribution of all the particles under consideration, only the distribution of some of their clumps in a simplified manner. We will get some numerical results in both cases, although some difficulties may arise. For example, when modeling the gases flow and heat exchange between them in a certain subregion, they are classified as constant in terms of parameters at an instant of time, some particles may be missing due to the simplified modeling for their movement, which is obviously not true due to their number and chaotic distribution.

To summarize, we can say that the generalization of the model to the case of interest to us, can be made by transitioning to a dynamic formulation that considers the change in the parameters of the gas mixture over time; the main difficulty will be the correct connection of both stages of modeling the carbon black formation in the furnace production method. We will apply the methodology described above, to simulate the process of formation of carbon black in furnace production. A simplified model of the reactor is shown in Fig. 18.

We will set the length of the last section of the reactor l_4, assume an insignificant content of hydroxyl radicals in the combustion flame of natural gas, use acetylene as a raw material, take the heat-carrier gas supply flow rate equal to 93697 m^3/h, and the raw materials flow rate 0.6 m^3/h. For example, we will assume the following reactor dimensions: l_1=3 m, l_2=1.2 m, l_3=2.2 m, l_4=8 m, D_1=1.2 m, D_2=1.8 m, D_3=2.4 m. The change in parameters responsible for mass fractions and density over time can be relatively easily calculated by neglecting the change in gas densities, and taking them relatively constant over time due to the high temperatures in the reactor. The change in temperature is quite difficult to track, so we will assume that it changes exponentially over time, and slows down a little every second. Thus, we obtain the following change in the values of concentration (Fig. 19) and mass density (Fig. 20), described in a logarithmic scales in the time interval from 0 to 4.25. when solving the Cauchy problem numerically with zero initial data, we carry out calculations with double precision.

4.6 Optimization formulation for solving the inverse coefficient problem, using data from experimental studies of carbon black formation in the reactor

The model of carbon particle nucleation and growth is based on two ordinary differential equations describing the instantaneous formation of the number of particles N and their mass M (17). The model coefficients for each source term, corresponding to the mechanisms of carbon nucleation, coagulation, surface growth, and oxidation, will be determined using an optimization method for solving the inverse coefficient problem. The objective functions will be deviations of the specified two carbon quantities obtained from in-situ studies at characteristic values of the parameters of the raw material mixture, its evaporation products, and the gas-heat carrier in the reactor. The formulation of the inverse problem is then presented, and a genetic algorithm [63] is used to solve it by the optimization method. The direct problem of modeling the technical carbon formation process, consisting of the system of equations (17) and its numerical solution method (18), is schematically represented as follows: $\boldsymbol{V}(t) = \boldsymbol{Z}(\boldsymbol{X}_0, \boldsymbol{Y})$, where $\boldsymbol{V}(t)$ includes the vector of solutions to the equations (17) - $\boldsymbol{X}(t)$ and other parameters characterizing the process; $\boldsymbol{Z}$ is the mathematical model of the process and its implementation method. The input parameters of the direct problem include the model coefficients $\boldsymbol{Y} = (y_1, \ldots, y_M)$, the vector $\boldsymbol{X_0}$, and the time t. We will denote all these input parameters as $\boldsymbol{x} = (x_1, \ldots, x_N)$. Thus, the direct problem can be formulated as follows: $\boldsymbol{V}(\boldsymbol{x}) = \boldsymbol{Z}(\boldsymbol{x})$. We will denote the required values of the vector $\boldsymbol{V}$ as $\boldsymbol{V}^*$ and set $\boldsymbol{F}(\boldsymbol{x}) = \boldsymbol{V}^* - \boldsymbol{Z}(\boldsymbol{x}) = (F_1(\boldsymbol{x}), \ldots, F_L(\boldsymbol{x}))$, as the problem of achieving the required process characteristics $\boldsymbol{x} = \boldsymbol{Z}^{-1}(\boldsymbol{V}^*)$, it's solved by the optimization method for the inverse problem $\min_{\boldsymbol{x}} (|F_1(\boldsymbol{x})|, \ldots, |F_L(\boldsymbol{x})|)$. Thus, we arrive at a multi-objective optimization problem. It is necessary to find the parameter values $\boldsymbol{x} = (x_1, \ldots, x_N)$ consisting of $\boldsymbol{Y} = (y_1, \ldots, y_M)$, $\boldsymbol{X}_0$, and the time t that ensure the minimum values of the L functionals:

$$\min_{\boldsymbol{x}} \left(|F_1(\boldsymbol{x})|, \ldots, |F_L(\boldsymbol{x})|\right), \qquad \boldsymbol{x} = (x_1, \ldots, x_N) \in \boldsymbol{X} \subset \boldsymbol{E}_N, \tag{19}$$

with phase constraints:

$$\boldsymbol{X}_0 = \{\boldsymbol{x} : x_{L,i} \leq x_i \leq x_{R,i}\}, \tag{20}$$

and target constraints:

$$\varphi_j(\boldsymbol{x}) \leq 0, \quad j = 1 = 1, \ldots, m.$$

To solve the problem (18)-(20), the Breeder Genetic Algorithm (BGA) is used, which is a stochastic multi-objective optimization algorithm [69-71]. In [63], it was shown that BGA is capable of quickly and reliably finding global optima of various functional dependencies. In [63], BGA was applied to solve a three-dimensional inverse problem of modeling water flows in various types of hydro turbines: Francis, Kaplan, and Pelton. The sought input parameters for the direct problem included the operating parameters of the hydro turbine, parameters defining its geometry, as well as the fluid parameters - the working body of the hydro turbine. The target functions were set as the extremes of efficiency coefficients, allowable loads on the structure, and weight values of the structure. The obtained results convincingly demonstrate the ability of BGA to find global optima.

The essence of BGA lies in forming an initial population of individuals – $\boldsymbol{x} = (x_1, ..., x_N)$. For each individual, the direct problem is solved $\boldsymbol{V}^k = \boldsymbol{Z}(\boldsymbol{x}^k)$. It is checked how well the found solution $\boldsymbol{V}^k$ meets the necessary conditions. If the conditions are not met, the next generation of individuals is created. The new generation is created based on the BGA command functions. After that, the calculations of the direct problem are repeated for the new generation until a generation of individuals giving the optimal solution of the problem in the form of a Pareto front is found. BGA command functions include: forming an initial population consisting of individuals $\boldsymbol{x} = (x_1, ..., x_N)$; calculating the values of target functionals $|F_1(\boldsymbol{x})|, ..., |F_L(\boldsymbol{x})|$ for each individual in the population; calculating the significance of each individual in the population; calculating a quality criterion based on significance for each individual; calculating the distances between individuals; calculating proximity numbers for each individual; calculating the quality function; selecting the best individuals for crossover; forming a new population through crossover; slightly modifying each individual in the mutation process; copying without modification all individuals meeting the constraints and rank 1 from the previous generation into the new generation. After copying, the size of the new generation will be $p + e$, where e is the number of copied individuals. The above commands are then repeated until the specified number of generations is calculated.

4.7 Test optimization problems

It is known [64], that the smaller the average diameter of carbon black particles, the greater the reinforcing property it has. In this case, the specific surface and the dispersion degree increases as well. In the model of the nucleation and growth of carbon particles, it is assumed that these particles have the shape of a sphere [53]. The volume of the ball is equal to $\pi d^3/6$, where d is the diameter of the ball. From here $M = \rho_{soot} N \pi d^3/6$ where M is the mass fraction of soot, N is the concentration of particles, $d = \sqrt[3]{6\pi M/(\rho_{soot} N)}$. The function $y = \sqrt[3]{x}$ increases monotonically, so we can take $F_1 = M/N$ as the first objective function and look for the input parameters of the carbon formation process model at which the average particle diameter will be minimal. And, therefore, the degree of dispersion will be maximum. We will take $F_2 = N$ as the second functional and will seek for obtaining as many carbon black particles as possible. We will pose three optimization problems.

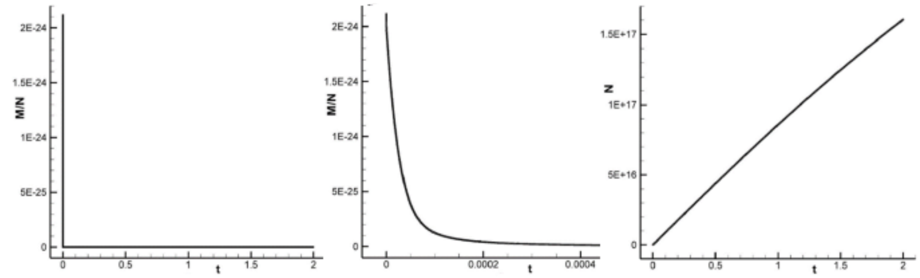

Figure 21: Dependence of $F_1 = M/N$ in the interval $0 \le t \le 2$ (left); fragment of F_1 in the interval $0 \le t \le 0.0004$ (center); dependence of $F_2 = N$ in the interval $0 \le t \le 2$ (right).

4.7.1 Problem 1

For given coefficients (α, β, γ, δ) of the model, determine the time point at which $\min F_1, \max F_2$ are obtained. Model coefficients (α, β, γ, δ) are specified according to formulas (10)-(14) with average values of gas parameters calculated according to the ranges of their changes (Tab. 4.2). The time limit is set: $0 < t < T$. Average values of gas parameters were taken as following: ρ=0.84, $Y_{C_2H_2}$=0.018, Y_{OH}=$1.2{\cdot}10^{-3}$, Y_{O_2}=0.039, T=1100. And with them, the coefficient of these models were calculated: $\alpha = 8.834{\cdot}10^{16}$, $\beta = 1.339{\cdot}10^{-13}$, $\gamma = 2.663{\cdot}10^{-6}$, $\delta = 8.242{\cdot}10^{-4}$. The graph of function $F_1 = M/N$ on the interval $0 \le t \le 2$, is shown in Fig. 21. There, we show a fragment of F_1 graph on the interval $0 \le t \le 0.0005$. Further more, we present the graph of function $F_2 = N$ at the time interval $0 \le t \le 2$. Genetic algorithm is applied for solving the optimization problem 1 (min F_1 and max F_2) with the presented objective function for an obvious solution, Pareto front which is shown in Fig. 22.

4.7.2 Problem 2

For the moment in time, found by solving optimization problem 1, find the model coefficients at which $\min F_1, \max F_2$ are obtained Limitations on the model coefficients (α, β, γ, δ) are determined using formulas (10)-(14) according to the ranges of changes in gas parameters (Tab. 4.1). The limitations on each coefficient is as following: $2.002{\cdot}10^5 < \alpha < 4.134{\cdot}10^{20}$, $9.032{\cdot}10^{-14} < \beta < 1.616{\cdot}10^{-13}$, $1.108{\cdot}10^{-13} < \gamma < 9.666{\cdot}10^{-4}$, $2.717{\cdot}10^{-5} < \delta < 1.140{\cdot}10^{-2}$. The solution of problem 2 is presented on Figs. 22-26.

4.7.3 Problem 3

For the given model coefficients (α, β, γ, δ) of problem 1, find the time point in interval $0 \le t \le 2$, at which min F_1 and min F_2 are obtained. The solution of problem 3 is presented on Fig. 27.

4.8 Results

After the overview of existing approaches to modeling the nucleation and growth of soot particles presented in the Introduction, the Moss-Brookes model of uncontrolled nucleation and growth of soot particles during acetylene combustion was chosen as the basis for the model of carbon black formation in the reactor. This model, on the one hand, stands out for its simplicity, and on the other hand, it has a theoretical basis unlike empirical models, which will allow further modifications to the model for a more accurate description of the technical carbon formation process. The model was analyzed. This semi-empirical model sufficiently describes the soot formation process but does not delve into the chemistry of the occurring processes, as the Frenklach M., Wang H. model does [31, 40]. The data obtained from the Moss-Brookes model most closely correspond to experimental data compared to the models of Tesner P.A. [23,37] and Khan I.M. [25]. It is important to note that reactions occurring in the combustion products of liquid hydrocarbons proceed much more slowly than

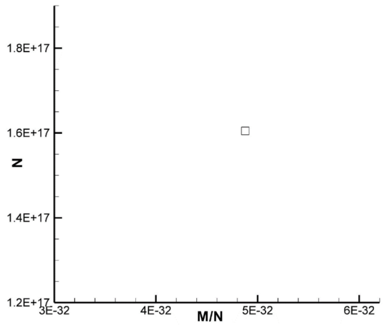

Figure 22: Pareto front for the functionals $F_1 = M/N$ and $F_2 = N$ for problem 1 (min F_1 and max F_2) – one point, $F_1 = M/N = 4.878 \cdot 10^{-32}$, $F_2 = N = 1.605 \cdot 10^{17}$, The values are reached at $t = 2$.

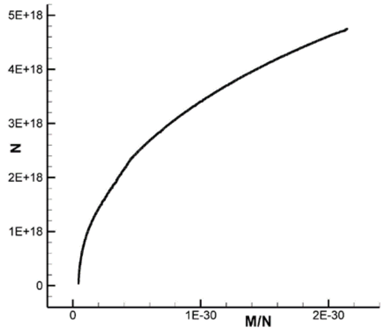

Figure 23: Pareto front for the functionals $F_1 = M/N$ and $F_2 = N$ for problem 2 (min F_1 and max F_2) at $t = 2$ for the specified variations of model coefficients.

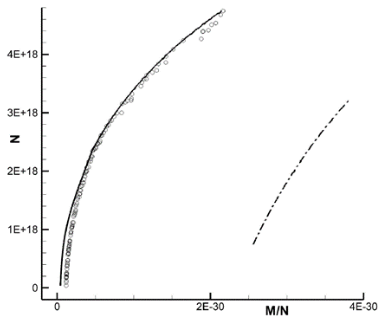

Figure 24: Pareto fronts for Problem 1: for $t = 1$ and $t = 0.1$, finding the gas parameters that ensure $\min F_1$ and $\max F_2$. Line – $t = 2$; circles – $t = 1$; dashed – $t = 0.1$.

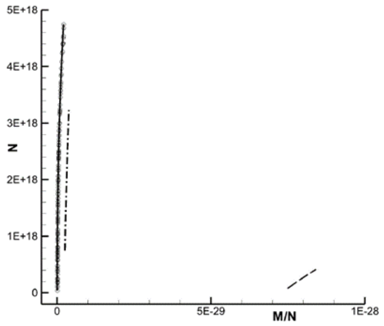

Figure 25: Pareto Fronts for Problem 2: for $t = 0.01$, finding the gas parameters that ensure $\min F_1$ and $\max F_2$. Line – $t = 2$; circles – $t = 1$; dashed - $t = 0.1$; dot-dashed – $t = 0.01$.

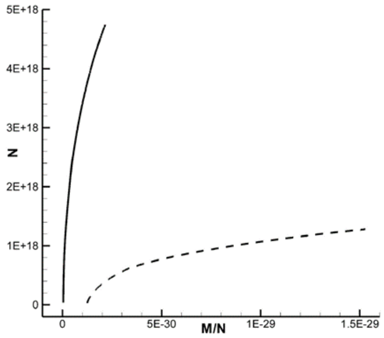

Figure 26: Pareto Fronts for Problem 3: for $t = 2$, find the remaining gas parameters that ensure $\min F_1$ and $\max F_2$ with a fixed $\rho_g as$. Solid line $\rho_g as = 0.84$; dashed line $\rho_g as = 0.085$.

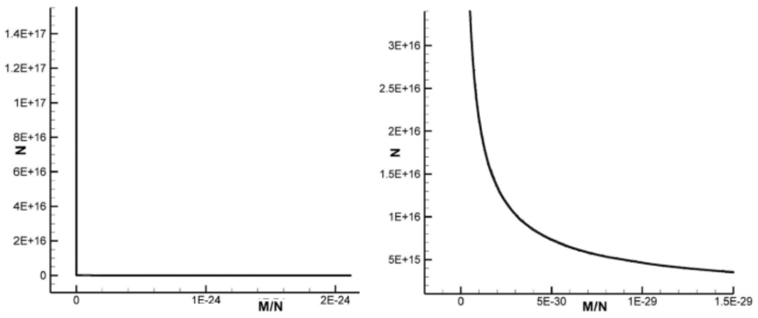

Figure 27: Pareto front for the functionals $F_1 = M/N$ and $F_2 = N$ for problem 3 (min F_1 and min F_2): the whole Pareto front (left); in the vicinity of zero (rigth).

reactions during acetylene combustion, so their modeling is separated. The Moss-Brookes model considers and finds two characteristic soot quantities: concentration and mass density, calculated inside the reaction chamber. As mentioned above, the model considers nucleation, coagulation, oxidation, and surface growth processes. The first two affect the concentration transfer process, while mass density is influenced by formation, oxidation, and surface growth processes. For reasonable simplification, acetylene is considered the main source of elementary carbon particles involved in formation and surface growth processes.

5 Conclusion

A classification of types of soot is presented, and indicated what place carbon black occupies in it, highlighting its characteristic parameters. The conditions for its furnace production in reactors and the requirements that must be observed and taken into account when modeling the production process are given. To solve the problem of determining the parameters of the raw material and injector that would ensure atomization of the raw material with the required surface diameter of the droplets, two numerical models were built that describe in a three-dimensional formulation the atomization and evaporation of liquid hydrocarbon raw materials in the flow of heat-carrier gas. The models are made in the approximation of the Eulerian-Eulerian approach, implemented on the FlowVision PC and ANSYS PC. In both options, the movement of the carrier phase (heat-carrier gas and raw material evaporation products) is described by a system of Navier-Stokes equations, taking into account turbulence, mass and heat transfer. To describe the dynamics of the dispersed phase, FlowVision PC uses convection-diffusion equations for particle concentration, momentum and phase energy. In ANSYS PC, the movement of the dispersed phase, as well as the carrier, is described by the Navier-Stokes equations. The disadvantage of the model on the FlowVision PC is the need to determine the concentration of particles at the entrance to the computational domain of the dispersed phase from the injector. Its advantage is that it is more economical than the model on the ANSYS PC.

A review of existing approaches to modeling the nucleation and growth of soot particles is presented. The model for the formation of carbon black in the reactor is based on the Moss-Brookes model of uncontrolled nucleation and growth of soot particles during the combustion of acetylene. Two approaches to generalizing this model to the case of carbon black formation in a reactor are discussed: based on the stoichiometric laws of material and heat balance; and on the solution optimization of the inverse coefficient problem, using data from experimental studies of the formation of carbon black in a reactor. Optimization problems have been formulated and solved to ensure that an optimal solution is found for obtaining carbon with the largest specific surface area, and, consequently, with the maximum degree of dispersion.

References

[1] Zuev V.P., Mikhailov V.V. (1965).*Soot production.* Moscow: Chemistry.

[2] Gulmisaryan T.G., Kapustin V.M., Levenberg I.P. (2017).*Carbon black: morphology,properties, production*, Moscow: Kauchuk and Rezina.

[3] Koshelev F.F., Kornev A.E., Bukanov A.M.(1978). *General rubber technology*,Moscow: Chemistry.

[4] Orlov V.Yu., Komarov A.M., Lyapina L.A.(2002). *Production and use of carbonblack for rubber*, Yaroslavl: Alexander Rutman.

[5] Aksenov A.A., Zhluktov S.V., Kashirin V.S., Sazonova M.L., Cherny S.G., Drozdova E.A., Rode A.A. (2023). *Numerical modeling in the FlowVision PC of spraying andevaporation of raw materials in the flow of coolant gas during furnace production of carbonblack*, Computer Research and Modeling, 15(4), 921-939. https://doi.org/10.20537/2076-7633-2023-15-4-921-939

[6] Aksenov A., Zhluktov S., Kashirin V., Sazonova M., Cherny S., Zeziulin I.,Drozdova E., Rode A.(2023). *Numerical modeling of raw materials atomization and vaporizationin a heat carrier gas flow in technical carbon production based on the Euler approach*, E3S Web of Conferences, 459, 04019. https://doi.org/10.1051/e3sconf/202345904019

[7] Tarraf D., Cherny S. (2023). *Comparative analysis of Euler models of multiphaseflows in the ANSYS software for the problem of spraying raw materials in a heat-carrier gasflow in the furnace production of carbon black*, E3S Web of Conferences, 459, 04059.

[8] Zeziulin I.V., Cherny S.G. (2024).*Three-dimensional model of the furnace productionprocess of carbon black from hydrocarbon raw materials.* Abstracts of the All-Russian Conference dedicated to the 105th anniversary of the birth of Academician of the Russian Academy of Sciences L. V. Ovsyannikova, "Mathematical problems of continuum mechanics" (May 13 - 17, 2024, Novosibirsk). SB RAS.

[9] Brookes S.J., Moss J.B. (1999).*Predictions of soot and thermal radiation propertiesin confined turbulent jet diffusion flames*, Combustion and Flame, 116, 486-503. https://doi.org/10.1016/S0010-2180(98)00052-6

[10] Gimaev R.N., Mukhamadeev E.Z., Galiev R.R.(2006). *Mathematical model ofthe process of obtaining low-active carbon black*,Bulletin of the Bashkir University, 2, 37-39.

[11] Palmer H.B., Cullis H.F., *The formation of carbon from gases* (1965). Chemistryand physics of carbon, (Vol. 1). New York: Dekker.

[12] Haynes B.S., Wagner H.G.(1981). *Soot formation*, Prog. Energy Combust. Sci., 7 , 229-273.

[13] Glassman I. (1988). *Soot formation in combustion processes*, 22-nd Symp (International) on combustion, p. 295-311.

[14] Bilger R.W. (1977). *Reaction rates in diffusion flames*, Combustion and Flame, 30, 277-284.

[15] Liew S.K., Bray K.N.C., Moss J.B. (1981). *A flamelet model of turbulent nonpremixed Combustion*, Combustion Science and Technology, 27, 69-73.

[16] Orloff L., De Ris J., Delichatsios M.A. (1987). *Chemical effects on molecularspecies concentration in turbulent fires*, Combustion and Flame, 69, 273-289.

[17] Sivathanu Y.R., Faeth G.M. (1990). *Temperature/soot volume fraction correlationsin the fuel-rich region of buoyant turbulent diffusion flames*, Combustion and Flame, 81, 150-165.

[18] Fletcher D.F. et al (1994). *Numerical simulations of smoke movement from apool fire in ventilated tunnel*, Fire Saf. J., 23, 205-325.

[19] Novozhilov V. et al (1997). *A computational fluid dynamics study of wood fireextinguishment by water sprinkler*, Fire Saf. J., 29.4, 259-282.

[20] Novozhilov V. et al (1997). *A computational fluid dynamic model of fire burningrate and extinction by water sprinkler*, Combustion Science and Technology, 123, 227-245.

[21] Yan Z., Holmstedt G. (1997). *CFD simulation of upward flame spread over fuelsurface*, Fire safty science, 5, 345-356.

[22] Novozhilov et al (1999). *Solid fire extinguishment by a water spray*, Fire Saf. J., 32.2, 119-135.

[23] Tesner P.A., Snegiriova T.D., Knoore V.G. (1971). *Investigating diesel engineperformance and emissions using CFD*, Combustion and Flame, 17, 253-260.

[24] Magnussen B.F., Hjertager B.H. (1977). *On mathematical modeling of turbulentcombustion with special emphasis on soot formation and combustion*, Symp. Int. Combust., 16, 719-729.

[25] Khan I.M., Greeves G., Probert D.M. (1971).*Prediction of soot and nitricoxide concentrations in diesel engine exhaust*, Air Pollut. Control. Transp. Engines. C., 142 , 205-217.

[26] Luo M., Beck V.A (1996). *Study of non-flashover and flashover fires in afull-scale multi-room building*, Fire Saf. J., 26 , 191-219.

[27] Moss J.B., Stewart C.D., Syed K.J. (1989). *Flowfield modelling of sootformation at elevated pressure*, Symp. Int. Combust., 22, 413-423.

[28] Syed K.J., Stewart C.D., Moss J.B. (1991). *Modelling soot formation andthermal radiation in buoyant turbulent diffusion flames*, Symp. Int. Combust., 23, 1533-1541.

[29] Leung K.M., Lindstedt R.P., Jones W.P.A (1991). *Simplified reactionmechanism for soot formation in nonpremixed flames*, Combust. Flame., 87, 289-305.

[30] Brookes S.J., Moss J.B. (1999). *Predictions of soot and thermal radiation propertiesin confined turbulent jet diffusion flames*, Combust. Flame., 116, 486-503.

[31] Frenklach M., Wang H. (1991). *Detailed modeling of soot particle nucleationand growth*, Symp. Int.Combust., 23 , 1559-1566.

[32] Yen A.C.Y et al (2021). *Multiphase CFD modelling for enclosure fires - Areview on past studies and future perspectives*, Experimental and Computational Multiphase Flow, 1-25. DOI: 10.1007/s42757-021-0116-4

[33] Ghose P. et al (2014). *Effect of air flow distribution on soot formation andradiative heat transfer in a model liquid fluid spray combustor firing kerosene*, International Journal of Heat and Mass Transfer, 74, 143-155.

[34] Novozhilov V. (2001). *Computational fluid dynamics modeling of compartmentfires*, Progress in Energy and Combustion Science, 27, 629-631. DOI: 10.1016/s0360-1285(01)00005-3

[35] Khan M., Greeves G.A (1974). *Method for calculating the formation and combustionof soot in diesel engines*, In: N.H. Afgan and J.M. Beer, editors Heat Transfer in Flames. Chapter 25 Scripta, Washington DC, 390-404.

[36] Magnussen B.F., Hjertager B.H.(1976) *On mathematical models of turbulentcombustion with special emphasis on soot formation and combustion*, In: 16-th Symp. (Int.) on Combustion. The Combustion Institute, 719-729.

[37] Tesner P.A., Snegiriova T.D., Knorre V.G. (1971). *Kinetics of dispersed carbonformation*, Combust. Flame., 17, 253-260.

[38] Brookes S.J., Moss J.B. (1999). *Prediction of soot and thermal radiation inconfined turbulent jet diffusion flames*, Combust. Flame., 116, 486-503.

[39] Hall R.J., Smooke M.D., Colket M.B. (1997). *Physical and chemical aspectsof combustion*, Gordon and Breach, 189-230.

[40] Frenklach M. (2002). *Method of moments with interpolative closure*, Chemical Engineering Science, 57, 2229-2239.

[41] Galanin M.P., Isaev A.V., Konev S.A. (2019). *On modeling of soot formationduring diffusion combustion of hydrocarbon fuels*, Preprints of the M.V.Keldysh Institute for Problems of Materials Science, 110, 32. DOI:10.20948/prepr-2019-110.

[42] Isaev A.V. (2005). *Identification of patterns of formation and gasification of dispersedcarbon by studying the combustion processes of hydrocarbon fuels in various conditions*, II International Scientific and Technical Conference, Aircraft engines of the XXI century. Moscow, CIAM.

[43] Isaev A.V. (1995). *Identification of patterns of combustion processes of hydrocarbonfuels through a comprehensive study of laminar diffusion flames*, Oil refining andpetrochemistry, 4, 14-18.

[44] Kokurin A.D., Vinogradov V.N. (1984). *Diffusion flame in technological processes*, Leningrad, LDNTP.

[45] Lapshin M.P. (2007). *Development of new technological solutions for the productionof furnace carbon black*, Dissertation for the scientific degree of Candidate of TechnicalSciences: 05.17.07 - chemistry and technology of fuels and special products. LLC "ResearchInstitute of Natural Gases and Gas Technologies - VNIIGAZ". Moscow.

[46] Chirkov D.V., Ankudinova A.S., Kryukov A.E., Cherny S.G., SkorospelovV.A. (2018). *Multicriteria optimization of the shape of a hydroturbine runner using efficiency,strength, and weight criteria*, Struct. Multidisc. Optim., 58, 627-640.

[47] Volkov R.S., Kuznetsov G.V., Strizhak P.A. (2016).*Influence of droplet concentrationon evaporation in a high-temperature gas*, International Journal of Heat and Mass Transfer, 96, 20-28.

[48] Schiller L., Naumann Z. (1935). *Ver. Deutsch. Ing.*, 77.

[49] Ranz W.E., Marshall W.R. Jr. (1952). *Vaporation from Drops, Part I*, Chem. Eng. Prog., 48.3, 141-146.

[50] Ranz W.E., Marshall W.R. Jr. (1952). *Vaporation from Drops, Part I and PartII*, Chem. Eng. Prog. 48.4, 173-180.

[51] Lee W.H. (1979). *A Pressure Iteration Scheme for Two-Phase flow Modeling*, Technical Report LA-UR 79-975. Los Alamos Scientific Laboratory, Los Alamos, New Mexico.

[52] Whitman W.G. (1923) *Chem. Met. Eng.* 29.

[53] Wen Z., Yun S., Thomson M.J., Lightstone M.F. (2003) *Modeling soot formationin turbulent kerosene/air jet diffusion flames*, Combustion and Flame, 135, 323-340.

[54] Young K.J., Stewart C.D., Moss J.B. (1994). *Soot formation in turbulent nonpremixedkerosine-air flames burning at elevalte pressure: Experimental measurement*, Twenty-Fifth International Symposium on Combustion, The Combustion Institute, Pittsburgh, 609-617.

[55] Brookes S.J., Moss J.B. (1999). *Predictions of soot and thermal radiation propertiesin confined turbulent jet diffusion flames*, Combust. Flame., 116, 486-503.

[56] Puri R., Richardson T.F., Santoro R.J. (1993). *Aerosol dynamic processes ofsoot aggregates in a laminar ethene diffusion flame*, Combust. Flame., 92, 320-333.

[57] Frenklach M., Clary D.W., Gardiner J., Stein S.E. (1984). *Detailed kineticmodeling of soot formation in shock tube pyrolysis of acetylene*, Twentieth Symposium (International)on Combustion, The Combustion Institute, Pittsburgh, 887.

[58] Harris S.J., Weiner A.M., Blint R.J. (1998). *Formation of small aromaticmolecules in a sooting ethylene flame*, Combust. Flame., 72, 91-110.

[59] Leung K.M., Lindstedt R.P., Jones W.P. (1991). *A simplified reaction mechanismfor soot formation in nonpremixed flames*, Combust. Flame., 87, 289-305.

[60] Neoh K.G., Howard J.B., Sarofim A.F. (1981). *Particulate Carbon FormationDuring Combustion*, Plenum, New York, USA.

[61] Lee K.B., Thring M.W., Beer J.M. (1962). *On the rate of combustion of sootin a laminar soot flame*, Combust. Flame., 6, 137-145.

[62] Kronenburg A., Bilger R.W., Kent J.H. (2000). *Modeling soot formation inturbulent methane-air diffusion flames*, Combust. Flame., 121, 24-40.

[63] Cherny S.G (2006) *Numerical modeling of flows in turbomachines*, S.G. Cherny, D.V. Chirkov, V.N. Lapin et al., Novosibirsk, Science.

[64] Ivanovsky V.I. (2004). *Carbon black. Processes and devices*, Textbook, Omsk, JSC "Techuglerod".

[65] Sorokin K.E., Zhluktov S.V., Aksenov A.A.(2021). *On the implementation ofthe Euler approach to modeling polydisperse media in the FlowVision software package*, Thermophysicsand Physical Hydrodynamics. Collection of abstracts of the VI All-Russian scientificconference with elements of the school of young scientists.

[66] Reitz R.D. (1987). *Modeling atomization processes in highpressure vaporizingsprays*, AST, 3, 309-337.

[67] Aksenov A.A., Zhluktov S.V., Kashirin V.S., Sazonova M.L., Cherny S.G., Zeziulin I.V., Kalugina M.D. (2024). *Three-dimensional Numerical Model of Kerosene Evaporationin Gas Turbine Combustors*, upercomputing Frontiers and Innovations, 10.4, 27-45.

[68] Khakimzyanov G.S., Cherny S.G. (2003) *Methods of Computations in 4 parts*, Textbook NSU, Novosibirsk. Part 1. Numerical Methods for Solving Cauchy's Problems for ODEs.

[69] Fonseca C.M., Fleming P.J. (1993). *Genetic Algorithms for Multiobjective Optimization: Formulation, Discussion and Generalization*, Proc. of the 5th Intern. Conf. on Genetic Algirithms, 416-423.

[70] Horn J., Nafpliotis N. (1993) *Multiobjective Optimization Using The NichedPareto Genetic Algorithm*, IlliGAL Report 93005, Urbana, University of Illinois.

[71] Goldberg D.E., Richardson J.J. (1987) *enetic algorithms with sharing for multimodalfunction optimization*, Proc. of the 2nd ICGA., NJ, 41-49.

[72] Fedorova N.N., Valger S.A., Zakharova Yu.V. (2016) *Modeling HydrogasdynamicProcesses in ANSYS 17.0: Textbook; Novosibirsk State University of Architecture and Civil Engineering.*

Cherny S. G.,
Kutateladze Institute of Thermophysics SB RAS,
pr. Lavrentyev 1, 630090 Novosibirsk, Russia,
Email: `sgcherny2023@yandex.ru`,

Zeziulin I. V.,
Novosibirsk State University,
Pirogova st. 2, 630090 Novosibirsk, Russia,
Email: `i.zeziulin@mail.ru`,

Tarraf D.,
Novosibirsk State University,
Pirogova st. 2, 630090 Novosibirsk, Russia,
Email: `d.tarraf@g.nsu.ru`,

Pochuev A. P.,
Novosibirsk State University,
Pirogova st. 2, 630090 Novosibirsk, Russia,
Email: `a.pochuev@g.nsu.ru`,

Boronenko I. S.,
Novosibirsk State University,
Pirogova st. 2, 630090 Novosibirsk, Russia,
Email: `i.boronenko@g.nsu.ru`

Received 08.08.2024 , Revised 15.01.2025, Accepted 20.02.2025, Available online 30.06.2025.